Investigating climate changes in East Africa during MIS5 using GDGTs from Lake Challa

Allix J. Baxter
Utrecht University, Faculty of Geoscience
Department of Earth Science: Earth, Life and Climate

Supervisor: prof. dr. Jaap Sinninghe Damsté
University of Utrecht, Faculty of Geosciences
Head of the Department of Marine Microbiology and Biogeochemistry,
NIOZ Royal Netherlands Institute for Sea Research

Universiteit Utrecht

0° N/S — DeepCHALLA — 250 kyr

NIOZ

Table of Contents

Abstract

Determining past continental climate variability is important for understanding Earth´s climate system, testing climate models and projections of anthropogenic climate change, and developing an environmental context for human evolution. Here I present a precipitation and temperature reconstruction for Eastern Equatorial Africa during the period 140 to 70 ka based on the relative abundances of lipid biomarkers (GDGTs) preserved in Lake Challa. This study confirms the occurrence of extended periods of severe aridity in tropical African during the last interglacial, termed African Megadroughts. The warmest temperatures during this interval occurred around 135 ka, and temperature recorded at Lake Challa shows similar trend to marine and ice core isotope records. Further, this study examines the presence of the so called H-Shaped GDGTs or GMGTs in Lake Challa and other East African lakes. In the East African lakes, there is a general trend of greater relative abundance of GMGTs in lakes with higher mean annual air temperature (MAAT). This thesis presents three new indices (Ratio 1, Ratio 2 and IR_{brGMGT}), based on the relative abundances of branched GMGTs in East African lake sediments, which show a strong correlation to MAAT. Using these indices to estimate past temperature changes at Lake Challa produces variable results.

Keywords: Lake Challa, African Megadrought, GDGT, Marine Isotope Stage 5.

1 Introduction

1.1 Background and aim of study

With the goal of developing a comprehensive understanding of Earth's dynamic climate history, climate records have been extracted from the ice sheets and the deep sea. While marine and ice core records form an integral part of our knowledge of the climate of the past, a lack of research from continental and equatorial sources can cause gaps in our understanding, as climate in these areas can be markedly different than the poles or oceans. Hence, there is a need for continuous paleoclimate reconstructions from a continental and equatorial context.

Tropical lakes sediments often have a high preservation of organic material and therefore have the potential to provide high resolution palaeoenvironmental reconstructions. Several lakes in Eastern Africa have been studied including Lake Tana (Costa et al. 2014), Lake Tangayika (Scholz et al. 2003; Felton et al. 2007), Lake Victoria (Stager et al. 1997), Lake Malawi (Scholz et al. 2007; 2011, Castañeda et al. 2009), Lake Turkana (Morrissey and Scholz 2014) and Lake Albert (Buening et al. 1997) and have added to our understanding of the global climate system during the Quaternary period. As Eastern Africa is the home of early humans, advancing our understanding of environmental changes in this area can also answer questions about early human evolution and migration, as human movement was limited by environmental factors, such as amount of rainfall. The expansion of early humans from Africa into the middle east and Eurasia is thought to have occurred around 100 ka (Grove et al. 2015). Several studies show that Eastern Africa experienced episodes of severe aridity termed "Megadroughts" around this

period (Scholz et al. 2007; Moernaut et al. 2010), which likely had a powerful impact on the ecology and biodiversity of the region (Cohen et al. 2007; Lyons et al. 2015).

Recently, over 200 meters of lake sediments were recovered from Lake Challa in Eastern Equatorial Africa. The composite core covers the last two glacial-interglacial cycles and the entire period of human evolution. Using lipid biomarkers preserved in the Lake Challa sediments, this thesis will discuss the timing and severity of the African Megadroughts and temperature history of Eastern Africa during the period 140-70 ka. This interval covers Marine Isotope Stage 5 (MIS5), or the last interglacial period.

In this introductory chapter, I will introduce the lipid biomarkers which I used to investigate the paleoclimate of Eastern Africa, and the progression of indices based on these lipids. Later in this chapter I will explain the drivers of African climate change on different timescales and what is known about the climate of Eastern African during the last interglacial. Finally, this chapter includes a description of Lake Challa and of the cores, and a summary of previous studies of Lake Challa.

1.2 Using GDGTs as paleoenvironmental indicators

By modifying the structure of cell membrane lipids, microbial populations can adjust the permeability and fluidity to minimize the loss of energy caused by ion diffusion across the membrane. Particularly, this is observed as a means of conserving energy under heat stress (Sollich et al. 2017 and references therein). Glycerol dialkyl glycerol tetraethers (GDGTs) are a group of membrane lipids produced by species of archaea and bacteria and are found abundantly in a variety of environments, including the oceans (Schouten et al. 2002), lakes (Powers et al. 2004), rivers (De Jonge et al. 2014b; Zell et al. 2013), estuaries (Castaneda et al. 2010), peats (Weijers et al. 2006a) and soils (Weijers et al. 2006b). The core lipids of GDGTs are preserved in sediments several millions years old and the distribution of certain GDGTs has been shown to relate to the environmental conditions under which they were produced (Schouten et al. 2013 and references therein). Therefore, GDGTs are widely used in paleoenvironmental research to investigate past climate changes. The main groups of GDGTs employed for paleoenvironmental reconstructions are isoprenoid GDGTs (isoGDGTs) and branched GDGTs (brGDGTs; see Fig. 1). By analyzing modern sediments, where the environmental conditions are known, studies have related the distribution of GDGTs to certain environmental parameters, such as temperature and pH.

1.2.1 isoGDGTs

IsoGDGTs are synthesized by different species of archaea and differ in the amount of rings incorporated into their alkyl chains (Fig. 1). The isoGDGTs used for climate reconstructions contain between zero and four cyclopentane moieties. The novel isoGDGT crenarchaeol (cren) and the crenarchaeol regio-isomer (cren′) contain four cyclopentane rings and an additional cyclohexane ring and are characteristic lipids of the ammonium oxidizing archaea *Thaumarchaeota* (Pitcher et al. 2011; Sinninghe Damsté et al. 2012b). The relative abundances of isoGDGTs can be used to investigate paleoclimate. Schouten et al. (2002) introduced the

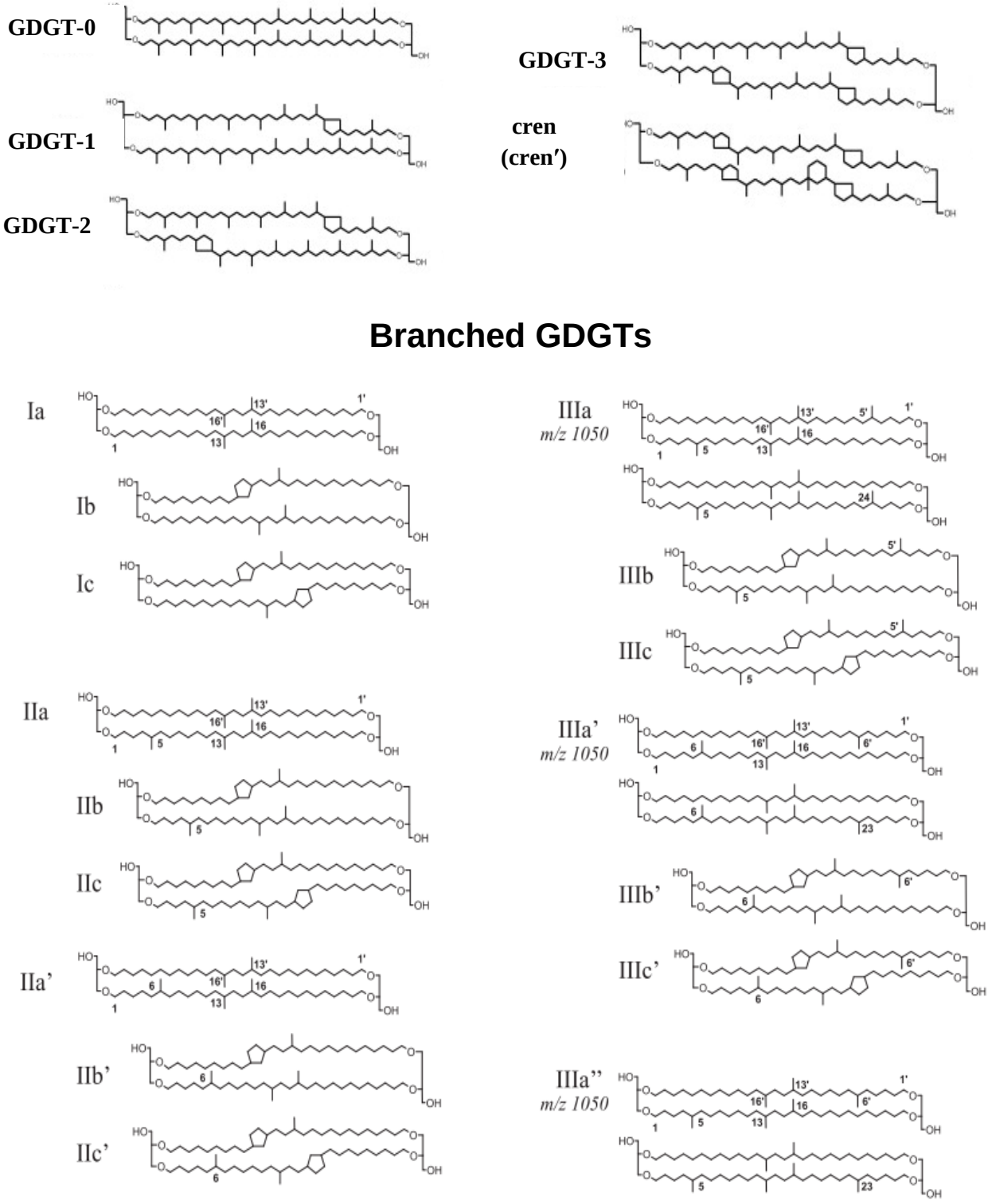

Figure 1: The stucture of the major iso and brGDGTs which are used in paleoclimate reconstructions. The image of the brGDGTs is taken from De Jonge et al. (2014,) and the image of the isoGDGTs is taken from Sinninghe Damsté et al. (2009).

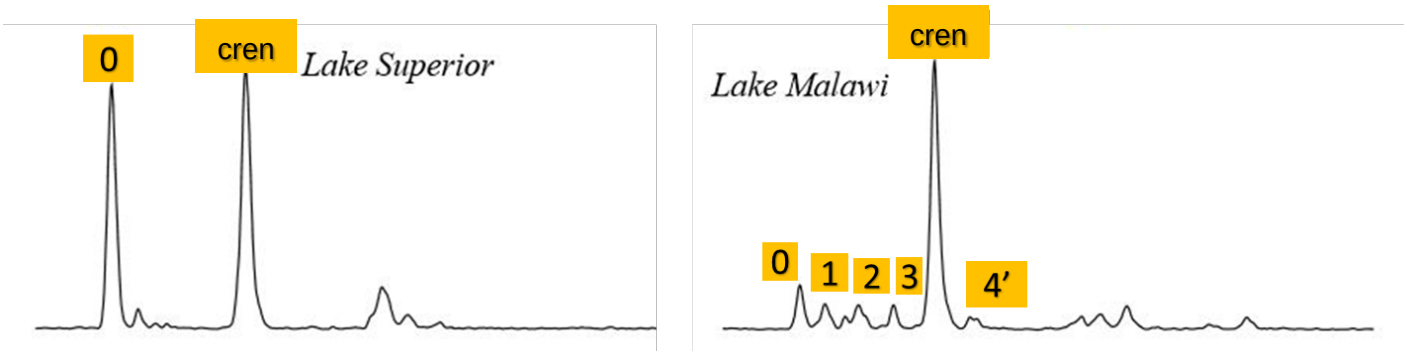

Figure 2. Mass chromatograms of polar fractions containing GDGTs from Lake Superior, a colder northern latitude lake, and Lake Malawi, a warm tropical lake. The lake sediments from Lake Malawi show greater amounts of GDGT-1,-2,-3, crenarchaeol and the crenarchaeol regio isomer relative to GDGT-0 than in Lake Superior. Image modified from Powers et al. (2004).

TetraEther IndeX of 86 carbons (TEX_{86}) paleothermometer, to estimate changes in sea surface temperature (SST) from ancient marine sediments. TEX_{86} is based on the observation that archaea produce greater amounts of isoGDGTs with more cyclopentane moieties at higher temperatures. TEX_{86} is calculated as the relative abundance of the isoGDGTs with two and three rings, and the crenarchaeol regioisomer, to the sum of all the lesser isoGDGTs (GDGT-1,-2, and -3) and the crenarchaeol regioisomer.

$$TEX_{86} = \frac{[GDGT-2]+[GDGT-3]+[cren']}{[GDGT-1]+[GDGT-2]+[GDGT-3]+[cren']} \quad (1)$$

In this way, it was recognized that larger TEX_{86} values correspond to higher temperatures. The TEX_{86} value is related to SST based on the established relationship between temperature and TEX_{86} calculated from globally distributed ocean core-top sediments (Kim et al. 2010). Although TEX_{86} was originally developed to reconstruct past changes in SST, it was proposed that the proxy can also be appropriately applied to large and deep lakes (Powers et al. 2004; 2005; see Fig. 2). This required the creation of alternative TEX_{86} temperature calibrations specific to lakes and several studies have done this using regional or global lake data sets. For example, using core top sediments, global lake calibrations were developed by Powers et al. (2010) and Pearson et al. (2011), and a calibration using European lakes was presented by Blaga et al. (2009). Further calibrations which focus more specifically on African lakes have also been refined and used to reconstruct past lake surface temperature variability, such as, for example at Lake Tanganyika (Tierney et al. 2010a). Castaneda and Schouten (2011) presented a combined calibration based on the data presented by Powers et al. (2010) and Tierney et al. (2010a).

1.2.2 brGDGTs

brGDGTs are produced by bacteria (most likely heterotrophic acidobacteria; Sinninghe Damsté et al. 2011; Weber et al. 2015) and are found particularly abundantly in soils and peat (Weijers et al. 2006a; 2006b). The main brGDGTs are tetra-, penta- or hexamethylated with zero to two cyclopentane moieties incorporated into their chains (Fig. 1). Weijers et al. (2007a) developed the Methylation of Branched Tetraether (MBT) and Cyclisation of Branched Tetraether (CBT) indices to express the environmental controls on the relative distribution of the particular membrane features.

$$\mathrm{MBT} = \frac{[\mathrm{Ia+Ib+Ic}]}{[\mathrm{Ia+Ib+Ic}]=[\mathrm{IIa+IIb+IIc}]+[\mathrm{IIIa+IIIb+IIIc}]} \quad (2)$$

$$\mathrm{CBT} = -\mathrm{LOG}\ \frac{[\mathrm{Ib}]+[\mathrm{IIb}]}{[\mathrm{Ia}]+[\mathrm{IIa}]} \quad (3)$$

As defined in Equation 2 above, higher MBT values indicate a greater relative abundance of tetramethylated brGDGTs (I), versus penta- (II) and hexamethylated (III) brGDGTs.

Weijers and colleagues (2007a) applied the MBT and CBT indices above to a globally distributed data set of 130 soils from 90 different locations. They used principle component analysis (PCA) to understand the factors controlling the variability of the particular brGDGTs. Their results suggested that CBT correlates with soil pH, with a lower cyclisation ratio corresponding to lower pH. They proposed that reduced membrane fluidity facilitated by greater membrane packing helps the bacteria survive in more acidic environments, as soil pH affects the proton gradient across the membrane (Weijers et al. 2007a). In contrast to what is observed in isoGDGTs, the cyclisation of brGDGTs was not found to show a relationship with temperature (Weijers et al. 2007a). However, the MBT index did show a positive correlation with mean annual air temperature (MAAT), although with a relatively large amount of scatter. A lesser degree of methylation was found to occur at higher temperatures. Furthermore, Weijer and colleagues (2007a) also found that MBT had a weak negative correlation with soil pH, with a greater amount of methylation corresponding to higher pH. The relationships between MBT and MAAT, and between CBT and soil pH as calculated by Weijers et al. (2007a) are shown in Equations 4 and 5.

$$\mathrm{MBT} = 0.122 + 0.187 \times \mathrm{CBT} + 0.020 \times \mathrm{MAAT} \quad (4)$$

$$\mathrm{CBT} = 3.33 - 0.38 \times \mathrm{pH} \quad (5)$$

The development of improved chromatographic techniques to investigate the relative abundance of GDGTs in sediments (Hopmans et al. 2016) led to the discovery that the isomers of the hexa- and pentamethylated brGDGTs with the additional methyl group occurring the sixth carbon position (6-me brGDGTs), had by the previous method been co-eluting with isomers which have the methyl group at the fifth carbon position (5-me brGDGTs; De Jonge et al. 2014a). As these brGDGTs are used in the CBT and MBT indices, the ability to separate the 5- and 6-methyl peaks in the mass chromatograms allowed for improvement of paleoclimate indices based on the distribution of brGDGTs. De Jonge et al. (2014a) therefore redefined the MBT and CBT indices to distinguish between the new and old method.

$$\mathrm{MBT'} = \frac{[\mathrm{Ia+Ib+Ic}]}{(\mathrm{Ia+Ib+Ic+IIa+IIa'+IIb+IIb'+IIc+IIc+IIIa+IIIa'+IIIb+IIIb'+IIIc+IIIc'})} \quad (6)$$

$$\mathrm{CBT} = -\mathrm{LOG}\ \frac{[\mathrm{Ib+IIb+IIb\prime}]}{[\mathrm{Ia+IIa+IIa'}]} \quad (7)$$

Equations 6 and 7 above are rewritten forms of the original MBT and CBT index to show explicitly that these studies used the chromatographic method in which the 5- and 6-methyl brGDGTs were coeluting. The 6-methyl isomers are indicated by the use of the prime symbol (eg. IIa′ in Equation 6). Equations 8 and 9 are new versions of the MBT and CBT indices based on only the 5 methyl GDGTs (De Jonge et el. 2014a). De Jonge et al. (2014a) reanalyzed a globally distributed soil data set (Peterse et al. 2012) using the new chromatographic technique and found that the greatest control on the fractional abundance of 6-methyl GDGTs appeared to be soil pH, and therefore was responsible for the dependence of the MBT index on soil pH. In addition, the fractional abundance of the 6-methyl brGDGTs showed a strong correlation with one another, which the authors speculate could suggests a common source organism. Thus, the removal of 6-methyl brGDGTs from the indices reduced the error of the CBT correlation to pH and the MBT correlation to mean annual air temperature (De Jonge et al. 2014a).

$$\mathrm{MBT'_{5ME}} = \frac{[\mathrm{Ia + Ib + Ic}]}{[\mathrm{Ia + Ib + Ic + IIa + IIb + IIc + IIIa + IIIb + IIIc}]} \quad (8)$$

$$\mathrm{CBT'_{5ME}} = -\mathrm{LOG}\ \frac{[\mathrm{Ib+IIb}]}{[\mathrm{Ia+IIa}]} \quad (9)$$

Because the brGDGTs were thought to be produced mainly in soils, previous studies have used the soil based brGDGT paleotemperature calibrations on ocean margin sediments (Weijers et al. 2007b), loess deposits (Peterse et al. 2011), and lake sediments (Fawcett et al. 2011). However, several studies now provide evidence for the production of brGDGTs within the water column of lakes, and report a significant differences between the brGDGT distribution found in lake sediments and surrounding catchment soils (Loomis et al. 2011; Sinninghe Damsté et al. 2009; Tierney and Russell 2009). Additionally, a novel hexa-methylated GDGT was discovered in surface sediments from a Swiss mountain lake, Lake Hinterburg (Weber et al. 2015). This isomer eluted between the 5- and 6-methyl brGDGTs and is named the 5/6-methyl brGDGT (IIIa″; Fig. 1), because it has additional methyl groups on the fifth and sixth carbon position (Weber et al. 2015). The authors found that this isomer was present in the lake sediments but not found in the surrounding catchment soils and had a strongly depleted δ^{13}C signal. Furthermore, the brGDGTs from the soils surrounding lake Hinterburg had significantly higher δ^{13}C values (difference of 16‰) than the brGDGTs present in the lake surface sediments, attesting to minimal terrigenous input and in situ production of brGDGTs in lakes (Weber et al. 2015). The soil based brGDGT calibrations, therefore, do not provide accurate temperature reconstructions when applied to lake sediments because the bacteria which produce brGDGTs in lakes and soils respond differently to temperature and chemical environment (Blaga et al. 2010; Russell et al. 2018).

Regional calibrations for East African lakes have been developed, which relate the distribution of brGDGTs found in recent lake sediments to environmental factors (Tierney et al. 2010b; Loomis et al. 2012; Russell et al. 2018). Recently, Russell et al. (2018) reanalyzed the East African lake

sediment data set published by Loomis et al. 2012, with the improved chromatographic method (Hopmans et al. 2016) allowing for the separation of the 5- and 6-methyl brGDGTS. They investigated a subset of 65 lakes with mean annual air temperatures ranging from 1.6 to 26.8°C and found that temperature was the dominant control on the variance of brGDGTs in East African lakes, including some of the 6-methyl brGDGTs. This is in contrast to earlier studies focusing on brGDGTs found in soil, where the fractional abundance of the 6-methyl brGDGTs is strongly linked to pH (De Jonge et al. 2014). Because of the weak correlation with brGDGTs, the pH calibration presented by the authors performed poorly.

Russell and colleagues (2018) created new calibrations for the MBT'_{5ME} and CBT'_{5ME} indices and additionally presented a new MAAT calibration (Eq. 10) which uses a stepwise forward selection (SFS) regression to select the brGDGTs which best predict MAAT (Equation 10).

$$\mathrm{MAAT} = 23.81 - 31.02*\mathrm{IIIa} - 41.91*\mathrm{IIb} - 51.59*\mathrm{IIb}' - 24.70*\mathrm{IIa} + 68.80*\mathrm{Ib} \quad (10)$$
$$(\mathrm{RMSE} = 2.14°\mathrm{C},\ R^2 = 0.94,\ p < 0.0001)$$

The SFS calibration in the paper using the new method produced an identical RMSE value to the Loomis et al. (2012) calibration which used the old chromatographic method. However, the Loomis et al. (2012) calibration underestimated the temperature of several of the largest lakes in Africa, whereas the SFS calibration presented by Russell et al. (2018) did not have this problem.

1.2.3 The BIT index

The Branched and Isoprenoid Tetraether (BIT) index was proposed as a novel proxy to trace the input of terrestrial material into marine environments (Eqs. 11 and 12; Hopmans 2004). It is calculated as the relative abundance of brGDGTs, presumably derived from soils, to the isoGDGT crenarchaeol, produced by the marine archaea *Thaumarchaeota*. In ocean and coastal locations, higher BIT values (closer to 1) represent a larger input of terrestrial organic matter into the marine environment.

$$BIT = \frac{[Ia+IIa+IIIa]}{[Ia+IIa+IIIa+cren]} \quad (11)$$

where GDGTs [Ia],[IIa] and [IIIa] are the brGDGTs and [cren] is crenarchaeol. The BIT index has also been rewritten by De Jonge et al. (2014a) to explicitly show the inclusion of the 6-me brGDGTs in the formula:

$$BIT = \frac{[Ia+IIa+IIa'+IIIa+IIIa\prime]}{[Ia+IIa+IIa'+IIIa+IIIa\prime+cren]} \quad (12)$$

In a study by Hopmans et al. (2004) the BIT index was applied to estuary surface sediments surrounding the Congo River Mouth to demonstrate how this proxy could be used to investigate fluvial transport of terrestrial material. Their results showed that BIT values were highest at the river mouth and decreased further into the Angola Basin. In lacustrine environments, the BIT index can be applied as proxy for rainfall. In this way, the flux of brGDGTs into lake sediments is

controlled by rainfall driven erosion of surrounding catchment soils into the lake, with increased rainfall leading to a larger concentration of the soil derived brGDGT in the lake sediments (Sinninghe Damsté et al. 2009). Thus causing higher BIT values to correlate with periods of greater precipitation in the past.

1.3 Tropical East African climate

1.3.1 Influences on East African climate

Equatorial Africa has a complex hydrological history and rainfall patterns have been shown to depend on many driving factors operating on different timescales. The precise location of Lake Challa makes it an ideal lake for paleoclimate reconstructions (Fig. 3). Firstly, Lake Challa is located just below the equator and therefore experiences two rainy seasons caused by the biannual passing of the Intertropical Convergence Zone (ITCZ), a narrow low pressure area where the trade winds converge, from March to mid-May and from late October to December (Buckles et al. 2016). Secondly, Lake Challa is located to the east of the Congo Air Boundary (CAB), a convergence zone which separates the area influenced by the Atlantic moisture source in the west from the area influenced by the Indian Ocean moisture source in the east (Tierney et al. 2011). The dominance of a zonal gradient (east to west) seems to be a reappearing feature in the hydrological history of equatorial Africa. For example, Tierney et al. (2011) found that, while previous research suggests dry conditions were present in Central Equatorial Africa during the Last Glacial Maximum, wet conditions prevailed in Eastern Equatorial Africa. This suggests that the behaviour of the CAB was driving this difference, rather than changes in the north-south direction caused by the ITCZ.

On inter-annual timescales, variability of the El Niño Southern Oscillation (ENSO) through its alteration of Indian Ocean sea surface temperature, impacts the movement of the ITCZ over Eastern Africa and therefore the amount of precipitation in this area (Wolff et al. 2011). The relationship between ENSO variability and rainfall in Eastern Equatorial Africa was inferred from a 3000 year varve thickness chronology from Lake Challa (Wolff et al. 2011). The variability of varve thickness in the record relates to the thickness of the diatom layer. The diatom layer is thicker for years which experienced prolonged windy conditions, which increase nutrient circulation in the lake system causing a diatom bloom. In the study they relate the thick varves to La Niña years, during which Eastern Equatorial Africa is dry and windy, and thin varves to El Niño years when the ITCZ remains over Lake Challa for a larger portion of the year and wetter conditions prevail.

In a study by Tierney et al. (2013) hydrological proxy data and coupled climate models were used to show that although on inter-annual timescales the influence of the tropical Pacific Ocean, which fluctuates in relation to ENSO, has a large influence on East African rainfall, on multidecadal timescales rainfall is predominantly controlled by the Indian Ocean variability. They promote that Indian Ocean variability controls East African rainfall by weakening or

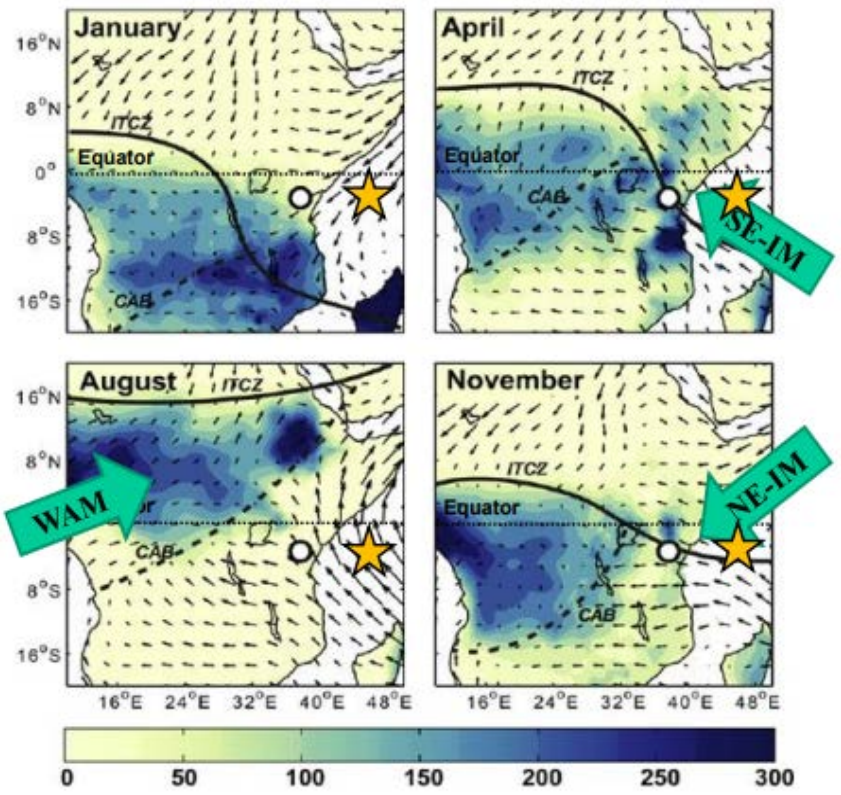

Figure 3. The position of Lake Challa (white dot) in earstern-most equatorial Africa which is always east of the Congo Air Boundary (CAB) and therefore cut off from the moisture source of the West African Monsoon (WAM). The migration of the Intertropical Convergence Zone (ITCZ) results in two rainy seasons (MAM and OND) separated by two dry seasons (JJAS and JF). The Northeasterly Indian Monsoon (NE-IM) and Southeasterly Indian Monsoon (SE-IM) deliver rainfall to the area of Lake Challa. Image modified from Tierney et al. (2011).

strengthening the local Walker circulation, linking lower SSTs in the eastern Indian Ocean and higher SSTs in the western Indian Ocean to wetter conditions in Eastern Africa.

Verschuren et al. (2009) used seismic reflection data and application of the BIT index to a 25,000 year record from Lake Challa to investigate the controls on the hydrology of Eastern Equatorial Africa. They found that on sub millennial timescales precipitation at the east African equator is related to changes happening in the northern high latitudes but on longer orbital timescales it responds more to low latitude insolation forcing. In the 25,000 year record, monsoon rainfall at Lake Challa varied at an 11,500 year periodicity caused by insolation forcing relating to a half precessional cycle. As the ITCZ passes over Lake Challa twice a year, a 'double frequency' in the rainfall signal appears. The north-easterly and south-easterly monsoons will be enhanced and Lake Challa will experience high rainfall, when the northern or southern tropics experience peak insolation (Verschuren et al. 2009).

1.3.2 East African Climate during the last interglacial-glacial transition

The last interglacial period corresponds to Marine Isotope substage 5e (MIS5e), also referred to as the Eemian, which occurred around 130 to 115 ka (Lisiecki and Raymo 2005). During MIS5e, global mean sea surface temperatures were at least 2°C warmer than preindustrial (Folland et

al. 2001; Otto-Bliesner et al. 2006). After this period global temperatures generally decreased as the climate transitioned into the most recent glacial period. Previous research found that variability in terrestrial temperature and precipitation records from across Africa during the interval 150-30ka is explained mostly by local insolation maxima, particularly during 150-75ka when the intensity and variability of radiation was extreme (Blome et al. 2011). Changes in temperature and precipitation in terrestrial African records do not appear to be responding to North Atlantic SST forcing, e.g. the timing of the MIS boundaries (Blome et al. 2011). In contrast, variability of African SST records during the same interval is determined largely by North Atlantic SST (Blome et al. 2011).

In contrast to the research described above, preliminary research has found evidence for the influence of Northern Hemisphere insolation forcing at Lake Challa. Previously, a low resolution temperature reconstruction for Lake Challa from present to 250 ka was created using the method based on the distribution of brGDGTs developed by Russel et al. (2018. Eq. 11; Sinninghe Damsté and Verschuren, unpublished). In the results from the preliminary study, the timing of variations in the MAAT record was comparable to changes in the isotope records from

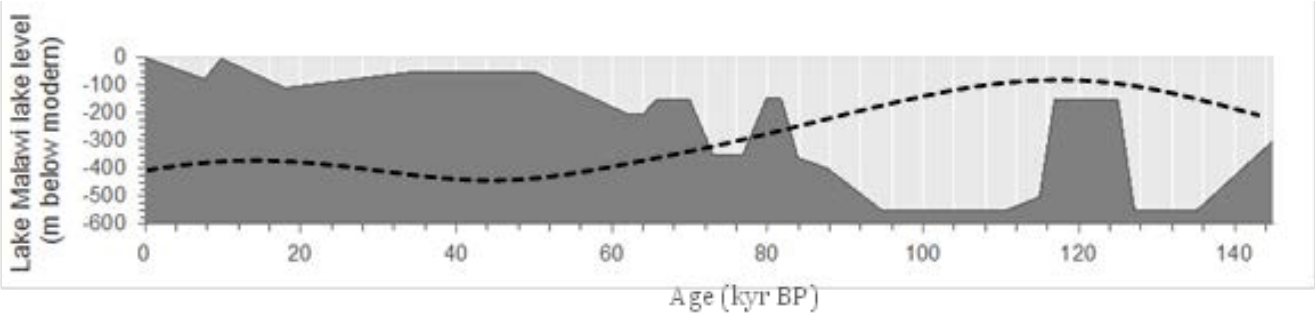

Figure 4. Lake level recontruction of Lake Malawi for the last 140 kyr, based on seismic reflection data (Scholz et al. 2007), shown with eccentricity (dashed line). Note that the age model presented by Scholz has since been revised (Lane et al. 2013) and that ages older than 60ka presented by the old age model, are shifted 10+kyrs older in the new age model.

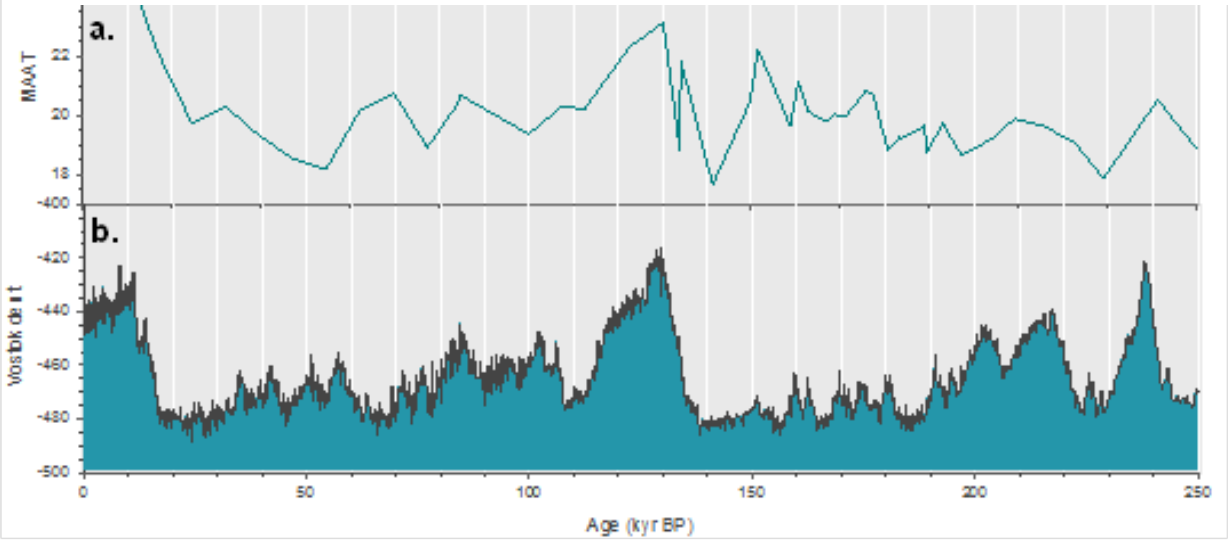

Figure 5. Plot (a) shows the unpublished results from a test study by, Sinninghe Damsté and Verschuren which shows a temperature reconstruction for the last 250,000 years based on the distribution of brGDGTs in Lake Challa (Eq. 10; Russel et al 2018). Plot (b) is a graph of the deuterium record from the Vostok core, Antarctica (Lorius et al. 1995).

the Vostok core and North Atlantic marine stacks (Fig. 5). Particularly, the timing of the last interglacial in the isotope records appears to correlate to warm temperatures at Lake Challa.

During this transition from interglacial to glacial conditions, the climate of tropical Africa is characterized by periods of severe aridity termed “megadroughts” which have been recorded in tropical lakes between ca. 80-115 ka (Blome et al. 2012). These megadroughts appear to be a specific feature of tropical African climate and are not evident in regions to the north and south of the African tropics (Blome et al. 2012). The evidence for African megadroughts was first presented by Scholz et al. (2007) in a 145 kyr lake level reconstruction for Lake Malawi (one of the African rift lakes that lies 10°S of the equator), based on seismic reflection data. The record shows a series of these severe droughts between 135 and 75 kya (Fig. 4). However, the exact timing the megadroughts recorded at Lake Malawi is somewhat poorly constrained, and the original age model presented by Scholz et al. (2007) has since been revised due to the identification of the Youngest Toba Tuff (YTT; dated to 75 ka) in the Lake Malawi core. The new age model differs from the previous age model by 10+kyrs at a depth of 28.10 meters (ca. 60ka by the previous age model). In the new age model, there is no age control in the interval between 75 ka and 590 ka, and it is possible that the actual timing of the megadroughts is not precisely resolved in the new age model.

Immediately north of Lake Malawi, evidence for an African megadrought during MIS5 was also found at Lake Tanganyika (the largest of the African rift lakes; location: 3-9° S; Burnett et al. 2011). Based on core stratigraphy and chemical analyses researchers determined that a period of intense aridity occurred sometime prior around 100 ka, although the exact timing and duration of which are difficult to discern. The hiatus recorded in the core is consistent with a drop in lake level of over 400 m (Burnett et al. 2011). Still further north, at Lake Challa, seismic reflection data shows that severe aridity occurred immediately before 128 ka (corresponding to Heinrich Event 11 in the North Atlantic) and between 114-97 ka during the Last Interglacial (Moernaut et al. 2010). Therefore, while moist and stable conditions were present in eastern tropical Africa from 97 ka to 20.5 (Moernaut et al. 2010), further south at Lake Malawi arid conditions prevailed until around 70 ka (Scholz et al. 2007). Notably, the arid conditions at Lake Challa appear to be more severe during the lake interglacial than what occurred during the Last Glacial Maximum (LGM; Moernaut et al 2010).

Evidence for megadroughts also comes from Western Tropical Africa at Lake Bosumtwi in Ghana. Seismic reflection data of a core from Lake Bosumtwi reveals a nonconformity which suggest the complete dessication of the lake around 80 ka, before lake level rose dramatically after 70 ka (Scholz et al. 2007). The megadroughts during this interval appear to be a universal feature of tropical African climate.

Scholz and colleagues (2007) explained the occurrence of megadroughts in the Malawi record as the consequence of failure of the precession driven monsoon in the southern tropics. However, at Lake Challa at the equator this would not be expected because of the opposing variability of the North and South monsoon. Therefore, the occurrence of a megadroughts in the Lake Challa record suggests the failure of both the northeasterly and southeasterly monsoons

during this interval (Moernaut et al. 2010). The extreme megadroughts in tropical Africa had a severe impact on the biodiversity of aquatic and terrestrial ecosystems and the return to a moist climate in eastern Equatorial Africa at 97 ka would have helped to maintain biodiversity in this area (Cohen et al. 2007). High latitude variability, such as the D-O events and Heinrich in the North Atlantic, and Indian Ocean SST had a significant influence on East African climate after 60 ka (Scholz et al 2007; Moernaut et al. 2010).

1.4 Lake Challa

Lake Challa is a 92 meter (in 2005) deep crater lake located at the base of Mt Kilimanjaro in Eastern Equatorial Africa (3°19'S, 37°42'E; 880 m above sea level; Verschuren et al. 2009). The catchment area of the lake is confined to 1.38 km^2 by high crater walls. During periods of exceptionally rain, the activation of the small ravine in the northwest corner of the lake can cause the catchment area to expand 1.43 km^2 (Buckles et al. 2014). Eighty percent of the hydrological input into Lake Challa comes from groundwater which originates as rainfall on the forested slope of Mount Kilimanjaro (Buckles et al. 2016). The amount of rainfall at Lake Challa is characterized by the biannual passing of the Intertropical Convergence Zone (ITCZ) which leads to two rainy seasons from March to mid-May and from late October to December (Verschuren et al. 2009). Lake Challa has a year round mixing depth of 15-20 m and between June and September deep mixing extends to 45-60 m deep (Sinninghe Damsté et al. 2009). Lake Challa has permanently anoxic bottom waters (Buckles et al. 2014) which leads to the high preservation or organic material, making Lake Challa and ideal site for paleoclimate reconstruction using organic biomarkers. As a tropical and continental record, the Lake Challa data has the potential to form an important complement to the large scale marine and ice core climate records from higher latitudes.

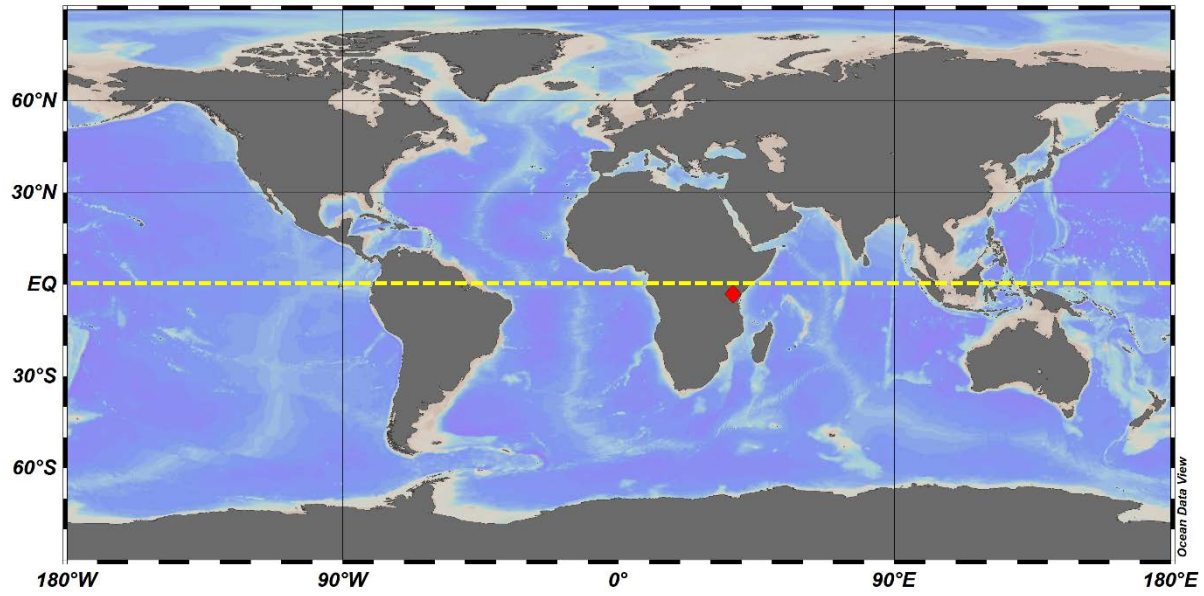

Figure 6. Location of Lake Challa (red diamond; 3°19'S, 37°42'E) just below the equator (yellow line).

Figure 7. Image of sections of the Lake Challa core (IDCP website; https://www.icdp-online.org/projects/world/africa/lake-challa/)

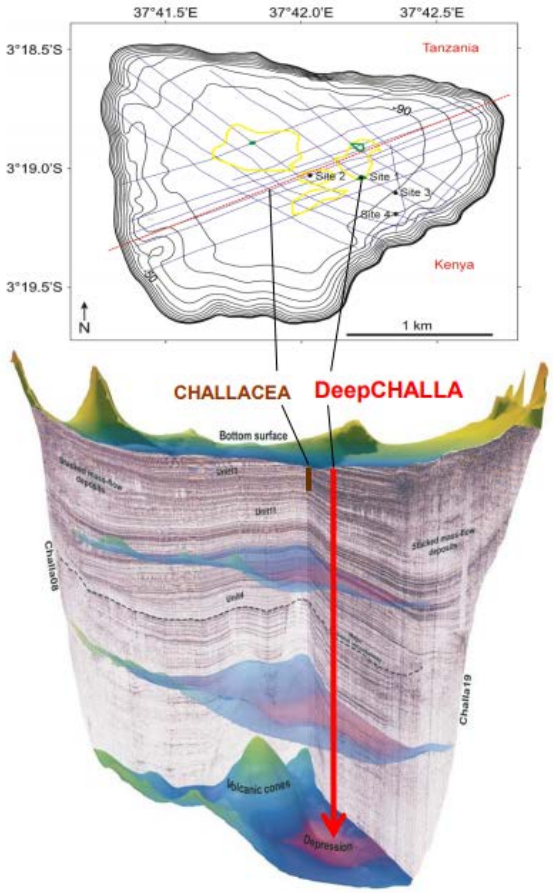

Figure 8. Location and depth of the CHALLACEA and DeepCHALLA cores within Lake Challa (Verschuren et al. 2013)

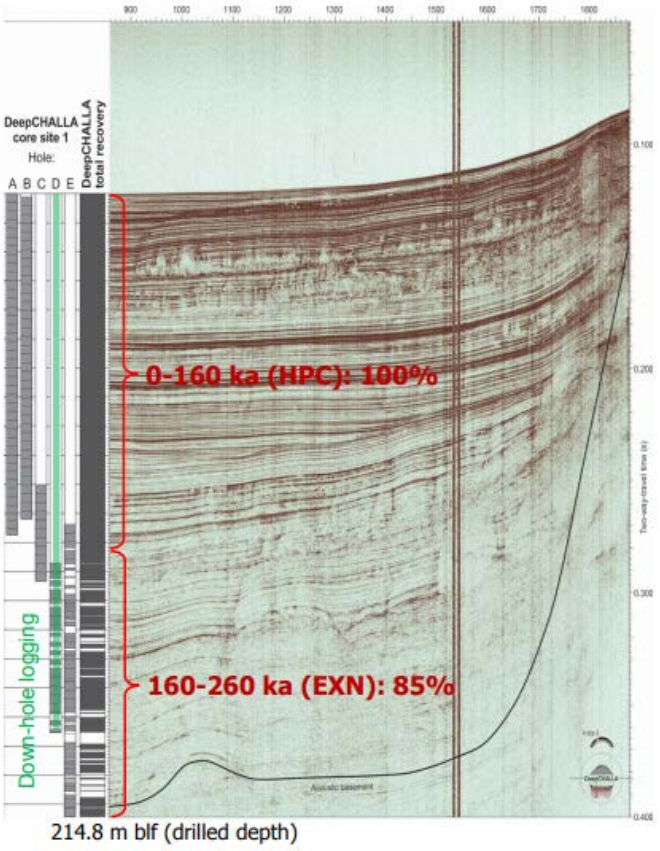

Figure 9. The depth of the DeepCHALLA cores (A-E) shown with the seismic profile of Lake Challa (Moernaut et al. 2010).

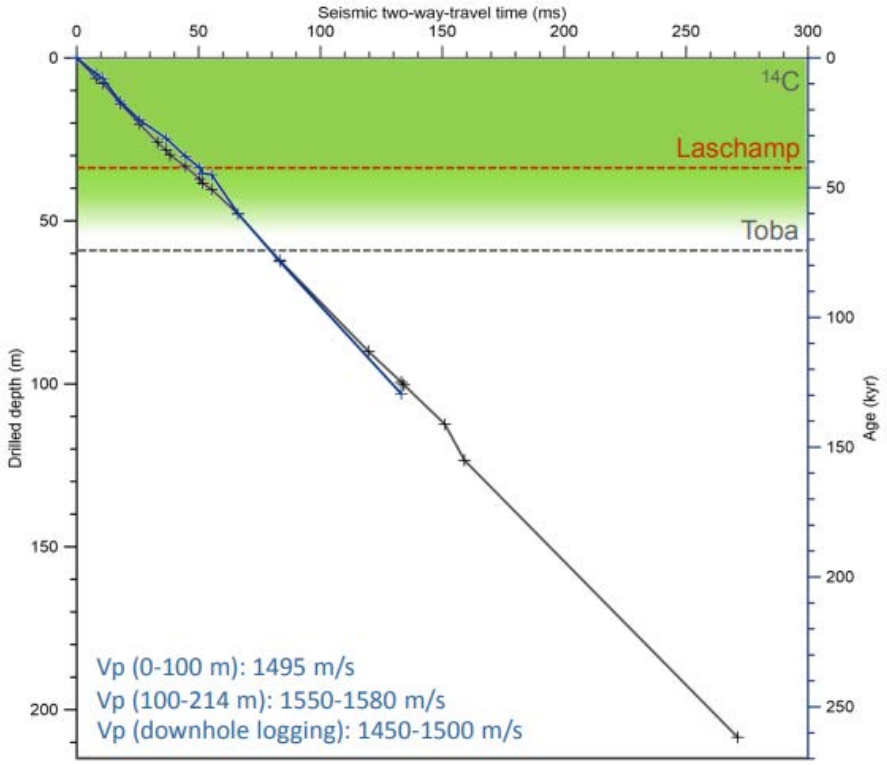

Figure 10. Preliminary age model for the DeepCHALLA core. For the first 140 kyr the based on seismostratigraphy from Moernaut et al. (2010), with tie points between certain sedimentological features. The age model is extrapolated for the rest of the series, with evidence suggesting very little compaction with depth.

1.4.1 Project DeepCHALLA

In 2016, as part of the International Continental Scientific Drilling Program (ICDP) project 'DeepCHALLA' (Verschuren et al. 2013), a sediment record of Lake Challa down to 214.8 meters below the lake floor was recovered, with 100% recovery in the uppermost 121.3 meters (the last ca. 160,000 years) and 85% recovery of the lower section (see Figures 8 and 9). The composite record covers the last 260,000 years, including the two most recent glacial-interglacial cycles, and is composed mainly of finely laminated lake sediments. The lowermost distinct reflector of the seismic stratigraphy is a unit consisting of volcanic sand and silt which was deposited around 260,000 years ago, and lies above older unsampled lake sediments (Verschuren et al. 2013). The individual cores are linked by tie points based on sedimentary features (mainly turbidites) to create the final composite core. The preliminary age model of the DeepCHALLA composite core (Fig. 10) is based on seismic stratigraphy for the first 140 ka period and extrapolated for the rest of the core as down-core compaction is minimal (Moernaut et al. 2010).

1.4.2 GDGTs in Lake Challa

As part of the ESF Euroclimate project CHALLACEA, several previous studies have analyzed the distribution of GDGTs from sediment traps placed in Lake Challa, the surrounding catchment soils, and also from a shorter cores. The BIT index reconstructed from the CHALLACEA core

spanning the last 25 kyrs shows a close correspondence to the Lake Challa lake level record (Verschuren et al. 2009; Fig. 11). Generally, highstands in Lake Challa correspond to periods of higher BIT values, and lowstands to lower BIT values. The lowest BIT values (around 0.3) occur during the LMG and Younger Dryas Stadial. The correspondence between BIT and lake level is in line with the rationale behind the BIT proxy: that periods of increased rainfall lead to a greater inclusion of soil derived brGDGTs into the lake sediments and thus a higher BIT.

The fractional abundances of core lipid (CL) GDGTs and intact polar lipid (IPL) GDGTs (representing the "living" microbial population) from the sediment trap data from Lake Challa provides us with detailed information about the seasonal fluxes and abundances of GDGTs into the lake system and about the sources of brGDGT. Sediment trap data was collected from Lake Challa on a near monthly basis from November 2006 to November 2007 (Sinninghe Damsté et al. 2009) and from December 2007 to August 2010 (Buckles et al 2014). brGDGTs and isoGDGTs were identified in the catchment soils, the water column, and the lake sediments (Buckles et al. 2014; Sinninghe Damsté et al. 2009).

It is important to know what months the different GDGTs are most prolific in the lake to understand the origin of the temperature signal that the GDGTs record. The peak flux of crenarchaeol, signifying the *Thaumarchaeota* bloom occurs typically between January and March, following the phytoplankton bloom (Sinninghe Damsté et al. 2009; Buckles et al. 2013; Buckles et al. 2014). For one season, from January to March 2009, the crenarchaeol peak in Lake Challa was absent. Notably, this is the same season where IPL and CL of brGDGTs, which are typically low for most of the record, show a significant peak between November 2008 and February 2009 (Buckles et al. 2014). It was proposed that the annual bloom of *Thaumarchaeota* was suppressed by the unusually dry conditions which occurred in late 2008 and early 2009, and instead a bloom of brGDGT producing bacteria occurred (Buckles et al. 2014).

Although the BIT and lake level record for Lake Challa correlate as expected, evidence strongly suggests that brGDGTs in the lake sediments are not derived from soils but are produced in the

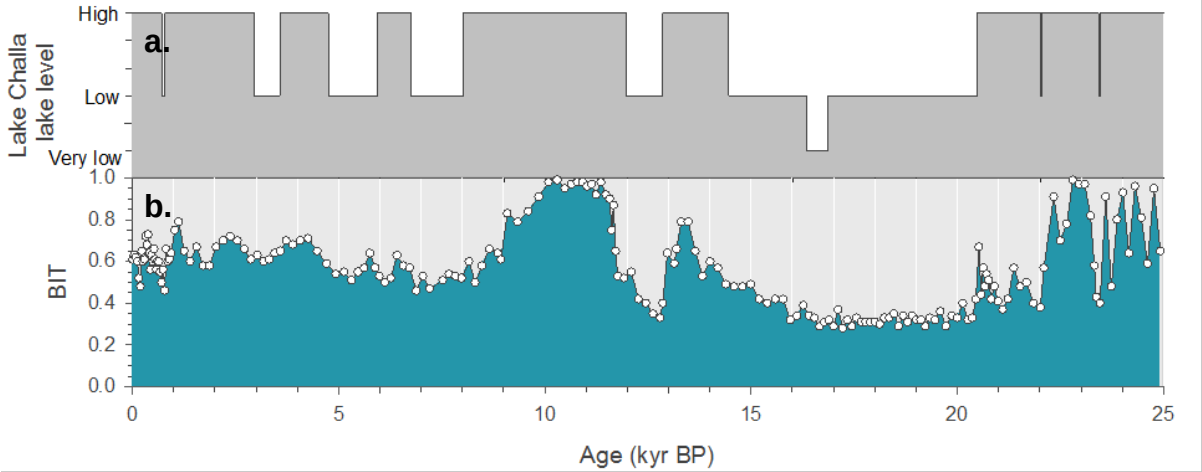

Figure 11. (a) Lake level reconstruction for Lake Challa based on seismic reflection dataplotted with (b) the BIT index for the last 25 kry at Lake Challa (Verschuren et al. 2009).

water column. Firstly, the concentration of brGDGTs in the lake sediments, both absolute and relative to C_{org}, were to two orders of magnitude higher than in the soils, and the percentage of IPL was also higher (Buckles et al. 2014). Furthermore, higher concentrations of brGDGTs did not appear in lake sediments near the lake edge or ravine mouth where the amount of erosion is expected to be greater, and BIT values of the soil were relatively low compared the BIT levels of the lake sediments (Buckles et al. 2014). As observed in other lakes (Tierney and Russel 2009; Loomis et al. 2011) the distribution of GDGTs is different between the soils and surface sediments of Lake Challa (Buckles et al. 2014).

As evidence strongly suggested in situ production of brGDGTs takes place in Lake Challa it was necessary to reexamine the relationship between rainfall and the BIT index. It was observed that the variability of the BIT index of the last 2200 years at Lake Challa has a strong negative correlation with the fluctuations in the concentration of crenarchaeol, and not of the brGDGTs (Buckles et al. 2016). Therefore, the correspondence of the Challa BIT record to precipitation history must emerge from a type of indirect relationship, as discussed by Buckles et al. (2016). They suggest that increased rainfall causes the introduction of nutrient rich organic matter into Lake Challa, which leads to a diatom bloom and therefore higher ammonium concentrations from the subsequent decay of organic material. *Thaumarchaeota* are nitrifiers (Buckles et al. 2013; 2016) and therefore should benefit from the ammonium created by the degradation of organic material. However, at high ammonium levels it has been shown that nitrifying bacteria outcompete nitrifying archaea). For Lake Challa, the BIT index is therefore a threshold indicator for precipitation and relates to high intensity precipitation events. Periods in the past with higher annual mean precipitation have a greater frequency of these events (Buckles et al. 2016).

2. Methods

2.1 Selecting of samples

The DeepCHALLA core was sampled in June 2017 at the University of Ghent. Work for this thesis took place at the Royal Netherlands Institute for Sea Research (NIOZ) in September of 2017 to March of 2018. A selection of 104 equally spaced samples covering the period from 140 to 70 ka were chosen resulting an average resolution of 650 years between samples (see Appendix 1). Samples were freeze-dried and homogenized with a mortar and pestle.

2.2 Sediment analysis

The sediment (0.3-1.2g dry weight) was extracted using a Dionex accelerated solvent extraction (ASE) system using with a 9:1 v/v mixture of dichloromethane (DCM) and methanol (MeOH). An internal standard of 1µg of synthetic C46 GDGT was added to the total lipid extract. The lipid extracts were then dissolved in DCM/methanol (1:1, v/v), passed through a Na_2SO_4 column and dried under N_2 gas. The lipid extracts were separated into apolar, ketone and polar fractions using Al_2O_3 column chromatography with eluents of hexane/DCM (9:1, v/v), hexane/DCM (1:1, v/v), and DCM/methanol (1:1, v/v) respectively, and dried under N_2 gas. The polar fractions,

containing the GDGTs, were then redissolved in hexane/isopropanol (99:1, v/v) and filtered using a PTFE 0.45 µm filter.

The polar fractions were analyzed using ultra high performance liquid chromatography – atmospheric pressure chemical ionization / Time-of-Flight mass spectrometry (UHPLC-TOFMS) on an Agilent 1290 Infinity II UHPLC, equipped with automatic injector, coupled to a 6230 Agilent TOF MS and Mass Hunter software according to Hopmans et al. (2016). Separation of the GDGTs was achieved in normal phase using 2 silica BEH HILIC columns in series (150 mm x 2.1 mm; 1,7 µm; Waters Acquity) at a temperature of 25 °C. The injection volume was 5 µL or 10 µL. Compounds were isocratically eluted with 82% A and 18% B for the first 25 min, followed by a gradient to 35% B in 25 min and a linear gradient to 100% B in 30 min. A = hexane and B = hexane/isopropanol (90:10, v/v) and the flow rate was 0.2 mL/min. The conditions for the APCI source were identical to Schouten et al. (2007) and Hopmans et al. (2016). In addition, the fragmentor was set at 300 V. The TOF MS was operated in extended dynamic range mode (2 GHz) with a scan rate of 2 Hz. We assessed GDGT distributions by monitoring m/z 700 to 1400. GDGT peaks were integrated using the Agilent Masshunter TOF Quantitative Analysis program, within the mass range of 10 ppm accuracy and applying 5-point Gaussian smoothing for relevant [M+H]+ signals and comparing the peak area to that of internal standard according to Huguet et al. (2006).

In order to assess the compatibility of the results of this study with previous studies which used the HPLC-MSD methods (Schouten et al. 2007; Hopmans et al. 2016) to calculate GDGT abundances, reference samples described in the interlaboratory study by Schouten et al. (2009) were run alongside of the sample set. TEX_{86} and BIT values obtained for those standards fell within calibration error from the values historically obtained in our laboratory with the HPLC-MSD methods.

Additionally, four samples were also analysed by UHPLC- high resolution MS (HRMS) using an Agilent 1290 Inifinity I equipped with thermostatted auto-injector and column compartment coupled to a Q Exactive (Quadrupole Orbitrap hybrid MS) MS equipped with ion max source with APCI probe (Thermo Fisher Scientific, USA). This was performed in order to investigate the structure of a group of later eluting ether lipids by means of MS^2 fragmentation data. Positive-ion APCI setting were as follows: capillary temperature 200 °C, sheath gas (N2) 50 arbitrary units (AU); vaporizer temperature 400 °C; auxiliary gas (N2) 5 AU, corona current 2.5 µA, APCI heater temperature 400 °C; S-lens 100 V. Chromatography was identical as described above for the UHPLC-MS analyses (i.e., 2 silica BEH HILIC columns in series according to Hopmans et al. 2016). Ether lipids were analyzed with a mass range of m/z 600 to 2000 (resolution 70,000), followed by data dependent MS^2 (resolution 17,500), in which the ten most abundant masses in the mass spectrum (with the exclusion of isotope peaks) were fragmented successively (stepped normalized collision energy 15, 20, 25; isolation window 1.0 m/z). An inclusion list was used with a mass tolerance of 3 ppm, comprehensively targeting ether lipids described in literature. Identification was achieved by comparison of exact mass and fragmentation spectra to literature (e.g. Knappy et al. 2009; 2015; Liu et al. 2012; Naafs et al. 2018).

The addition of an internal standard (IS) to the Lake Challa samples allowed the absolute concentration of crenarchaeol to be determined for each sample. It was calculated as follows:

$$\text{ng/g of cren} = \frac{[(area\ cren_{sample})/(area\ IS_{sample})]*[(mass_{IS}(ng))/(mass_{sample}(g))]}{fractionation\ factor} \quad (13)$$

Where the fractionation factor refers to the (area cren/area IS) calculated from a laboratory standard containing equal masses of crenarchaeol and the internal standard.

2.3 Indices and calibrations

The TEX_{86} index (Eq. 7) was applied to this data series and wastranslated to LST using the calibrations of Powers et al. (2010; Eq. 14), Tierney et al (2010a; Eq. 15) and Castaneda and Schouten (2011; Eq. 16). Note that corrections of all three calibrations were presented by Castañeda and Schouten (2015) and that the equations given below are the revised calibrations.

$$LST = 55.781*TEX_{86} - 13.949 \quad (14)$$
$$LST = 39.541*TEX_{86} - 4.0133 \quad (15)$$
$$LST = 49.032*TEX_{86} - 10.989 \quad (16)$$

Further, MAAT was estimated using Equation 10 defined Russel et al. (2018) based on the distribution of brGDGTs. The BIT index as defined by Hopmans et al. (2004), shown in Equation 12 was also applied to this data series to investigate changes in past rainfall at Lake Challa.

2.4 Statistical analysis

Principal component analysis (PCA) of the fractional abundance of GDGTs was performed using the SigmaPlot 14.0 (Systat Software, Inc. 2017). PCA allows us to assess the possible common variance between the different GDGTs.

3. Results

3.1 Distribution of GDGTs and GMGTs in Lake Challa

The polar fractions of the Lake Challa samples were analyzed using ultra high performance liquid chromatography – atmospheric pressure chemical ionization / Time-of-Flight mass spectrometry (UHPLC-TOFMS). The mass chromatography of the polar fractions of Lake Challa samples show that all the samples contained ample amounts of iso and brGDGTS necessary for the use of GDGT based paleo indices. Immediately noticeable from the total ion current (TIC) chromatograms, representing the sum of all ion currents carried by the separate ions of different m/z, is the relative absence of crenarchaeol in some samples. Figure 12a shows an example of a TIC chromatogram for a sample which contains very low amounts of crenarchaeol, resulting in a BIT value of 0.99. Figure 12b, shows the other extreme; this sediment contains relatively large

amounts of crenarchaeol and has a BIT value of 0.09. The brGDGTs account for between 3.5% to 63.7% of the combined total of iso and brGDGTs present in the samples.

The TIC chromatograms from the Lake Challa samples revealed a cluster of significantly abundant and unidentified ether lipids which eluted around 20 minutes after the brGDGTs (Fig. 12, Fig. 13). These lipids have m/z 1020, 1034 and 1048, and often display an interesting distribution of isomers (Fig. 13). The ratio between the isomers is not consistent throughout all the samples. Often, the unknown GDGTs in the Lake Challa sediments are more abundant than the mono-cyclic branched GDGTs with the same [M+H]+, but never appear more abundantly than the acyclic brGDGTs in the samples. It was theorized that this group could represent branched H-shaped GDGTs (HbrGDGTs), also referred to as glycerol monoalkyl glycerol tetraethers (GMGTs). GMGTs are a lesser studied group of archaeal and bacterial lipids. Recent research has shown that they have potential to be used as paleoclimate indicators (Naafs et al. 2018). They are referred to as H-shaped GDGTs because their structure is similar to that of regular GDGTs but with a covalent carbon-carbon bond connecting the two alkyl chains (Fig. 14;

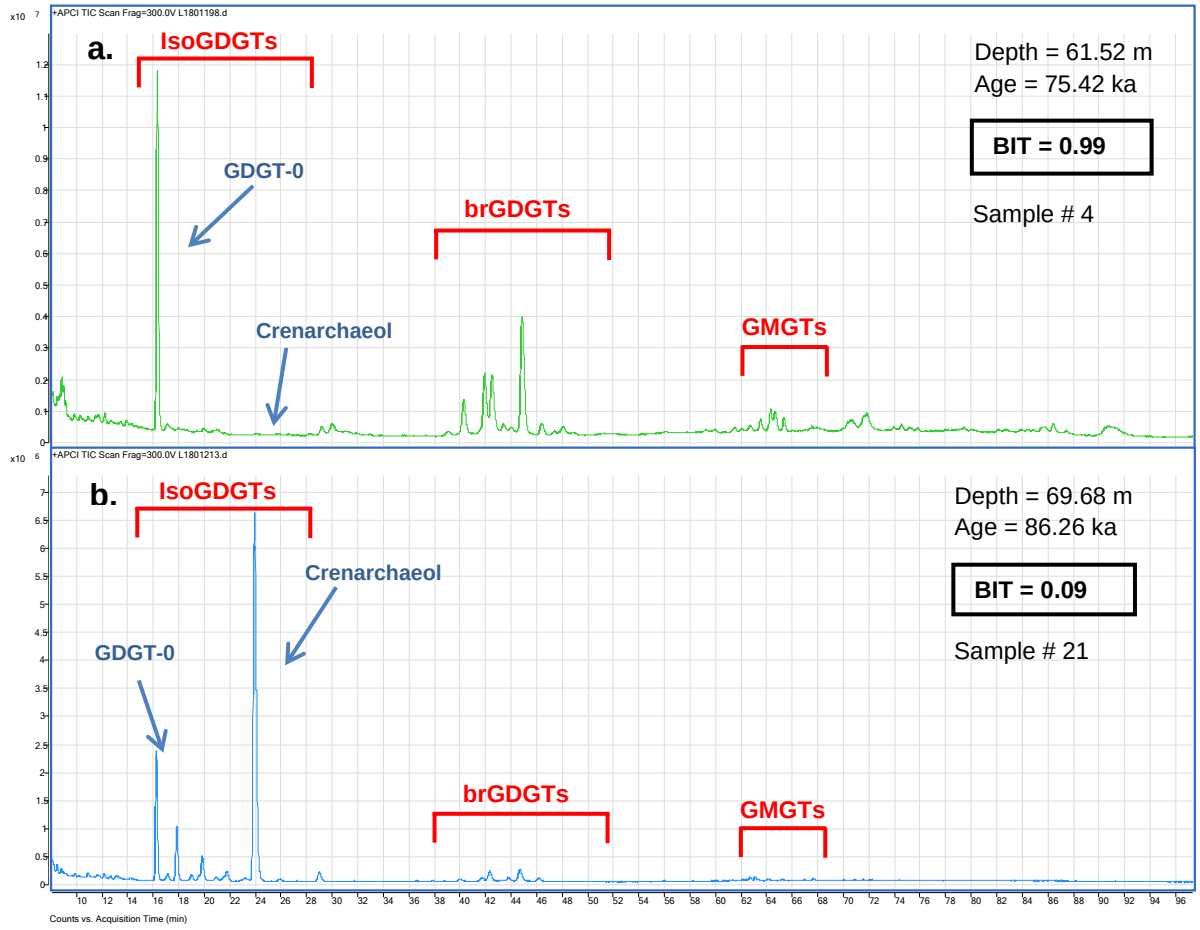

Figure 12. Example of total ion current (TIC) chromatograms of the polar fraction of the Lake Challa samples showing the extreme differences in the BIT index. Example (a) is a chromatogram with a BIT of 0.99, where the crenarchaeol peak appears almost absent (sample # 4; see Appenndix 1). Sample (b) is an example of a sample with a BIT value of 0.09, where crenarchaeol is abundant (sample # 21; see Appenndix 1). The relative abundance of brGDGTs is also variable amongst samples and a later eluting group of lipids called GMGT also appear in measureable amounts in the Lake Challa samples.

Naafs et al. 2018). The additional carbon-carbon bond causes GMGTs to be more polar than GDGTs, resulting in a longer retention. Both branched (brGMGTs) and isoprenoid GMGTs (isoGMGTs) have been identified (Knappy et al. 2009; 2015; Liu et al. 2012; Naafs et al. 2018), which have an [M+H]+ value of 2- than their GDGT homologue. Therefore, the brGMGTs with m/z values of 1020, 1034 and 1048 could represent homologues of the acyclic brGDGTs, Ia, IIa and IIIa respectively.

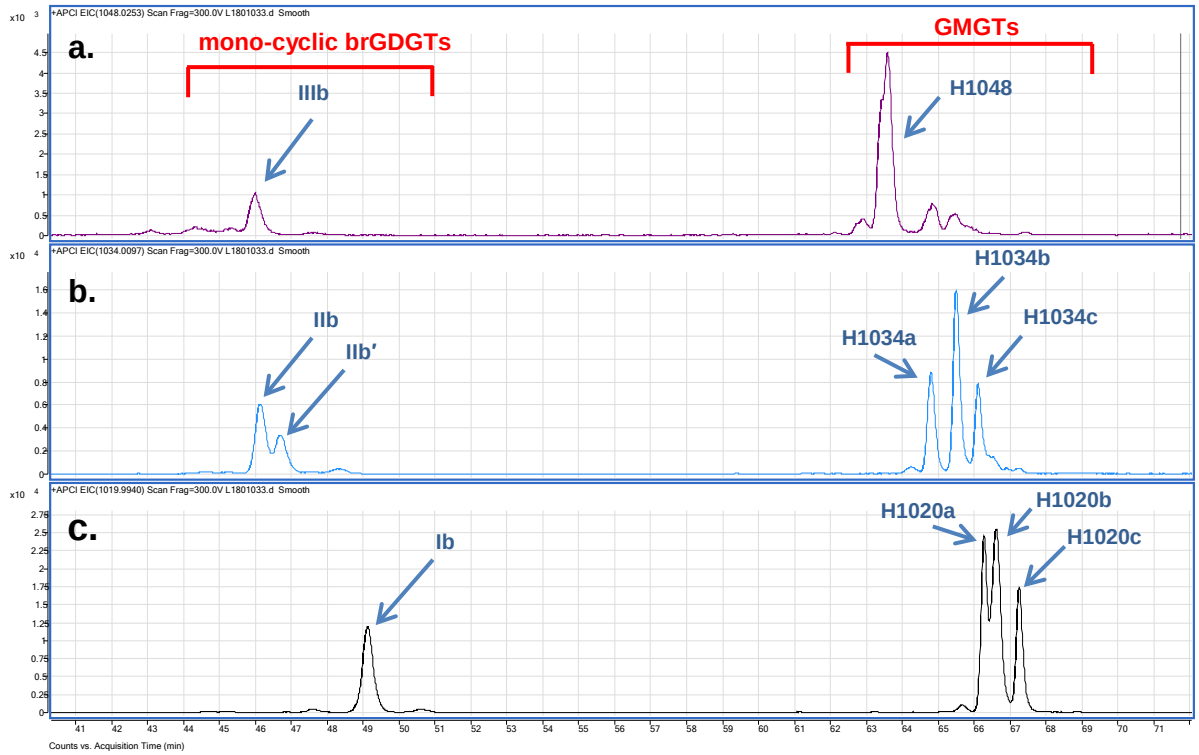

Figure 13. Mass chromatograms of sample #7 from Lake Challa (depth = 62.96 m, age = 77.2 kry BP) for (a) m/z 1048.025, (b) m/z 1034.0097 and (c) m/z 1019.9940 showing the regular mono cyclic brGDGT eluting before the later eluting group.

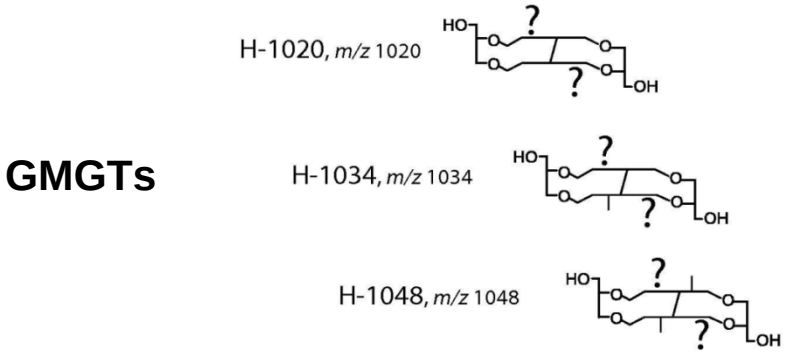

Figure 14. The theorised structure of H-1020, H-1034 and H-1048 GMGTs, also referred to as the H-Shaped brGDGTs. The position of the additional methyl groups and C-C bridge is unknown (image from Naafs et al. 2018).

Analysis of the fragmentation patterns of the unknown GDGTs confirmed their identity as GMGTs (Figs. 16-18). The MS^2 data of GMGTs show a distinctly different fragmentation pattern from that of GDGTs. The loss of one of the biphytanyl chains of GDGTs during collision induced dissociation (CID) results in products ion peaks in Region 3 (Fig. 16a), while the product ions of GMGTs only appear in Region 1 (Fig 16b). The C-C bond of GMGTs remains intact during CID, making the loss of a phytanyl chain impossible. Product ions in Region 1 relate to the loss of small neutral molecules from the terminal glycerol moieties (Knappy et al 2009; 2015). The individual present in the Lake Challa samples all showed the fragmentation pattern consistent with GMGTs. The position of the cross link in GMGTs is difficult to determine and still under debate (Liu et al. 2012; Naafs et al. 2018).

The fractional abundance of the nine major brGDGT (Ia, Ib, IIa, IIb, IIa′, IIb′, IIIa and IIIa′) and the brGMGTs isomers were calculated for the Lake Challa core samples. In the Lake Challa samples %GMGTs (defined as the contribution of all the brGMGT isomers, as labeled above, to the sum of the brGMGTs and major brGDGTs) ranges from 3.5% to 42.6%. Principal component analysis (PCA) was performed on the data set in order to better understand the controls on the abundance of the brGMGTs. The results of the PCA of the Lake Challa core samples show that the first three PCs account for 75% of the total variance. In the plot of PC1 versus PC2 (Fig 19a), the brGMGTs form a tightly grouped cluster, which load strongly positive on PC1 and show minimal loadings on PC2. The regular acyclic 5me-brGDGTs (Ia, IIa and IIIa) all also load positively on PC1, and brGDGT-Ia appears within the cluster of brGMGTs. In contrast, the 6me-brGDGTs (IIa′, IIb′ and IIIa′) load strongly negative on PC1. All the 5me-brGDGTs, with the exception of Ia, load positively on PC2. It is difficult to observe a pattern in PC3 (Fig. 19b).

3.2 Distribution of GDGTs and GMGTs in East African lakes

It would be expected that other African lakes also contain significant amounts of brGMGTs. Previously, modern surface sediments were collected from a number of East African lakes, mainly from Uganda and Kenya, and the abundances of GDGTs in the surface sediments were analysed (Russel et al. 2018). The East African lake data set includes lakes from a range of temperatures (MAAT=1.6-25°C) and altitudes (615-4752 masl), and has additional information about the lakes such as measured water temperature and pH values at different depths. For the purpose of this thesis, the HPLC-MS data from the East African Lake data set was reintegrated in order to inspect for brGMGTs. From most of the lakes (76) distinguishable amounts of GMGTs with the expected retention time and m/z values of the brGMGTs as seen in Lake Challa were identified. Thus, acyclic branched GMGTs appear commonly in East African lakes.

Not all of the East African lakes displayed the type of distribution of the brGMGTs as seen in Lake Challa. The individual isomers of the brGMGTs in the East African Lakes were identified and integrated as shown in Figure 15. The fractional abundance of the major brGDGT and brGMGT isomers was calculated and PCA was performed. In the East African Lake data set, the %GMGTs has quite a large range varying from 0.5% to 32%. In the PCA results for the East African lake data set, the first three PCs account for 73% of the total variance (Fig. 20). Again, all the brGMGTs load positively on PC1. PC2 separates the 6me- and 5me-brGDGTS, with 6me-

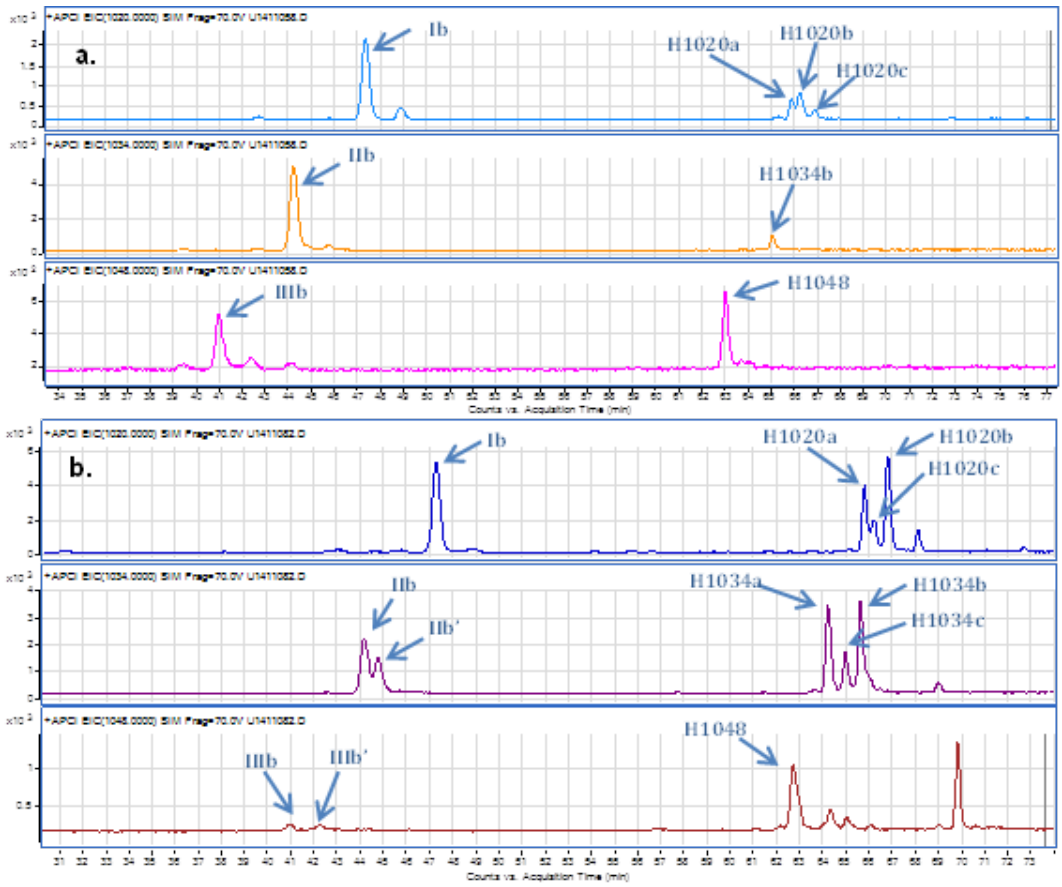

Figure 15. Mass chromatograms of the polar fraction of lake sediments extracted from (a) Lake Nanyunki Tarn, Kenya (Elevation = 4493 m: MAAT =5°C) and (b) from Lake Mirambi, Uganda (Elevation = 1075m: MAAT = 23.7°C)

brGDGTs loading strongly negatively on PC2. Further, PC3 appears to separate the cyclic from the acyclic GDGTs, and the brGMGTs group with the acyclic brGDGTs on PC3.

4. Discussion

4.1 GDGT ratios and environmental reconstructions

4.1.1 Rainfall and BIT record

The application of the BIT index to the lake samples allowed for the reconstruction of past rainfall variability at Lake Challa from ca. 140 to 70 ka (Figs. 21b, 23b). The magnitude of changes in the BIT record is extreme. For most of the time series the BIT index is low, <0.2, indicating extended periods of dry conditions in Eastern Africa from 138 to 128 ka, and from 118 to 80 ka, which will be referred to as the first and second megadroughts respectively. The timing of the first megadrought corresponds to the MIS6 glaciation, during which dry conditions are expected for in tropical Africa. The timing of the second megadrought in the lake Challa BIT index confirms the existence of the MIS5 megadrought. There are some slightly higher BIT values (around 0.3) after 100 ka, before the BIT index rapidly increases at 80 ka, suggesting wetter and more stable conditions. The two periods of intense aridity are separated by a period

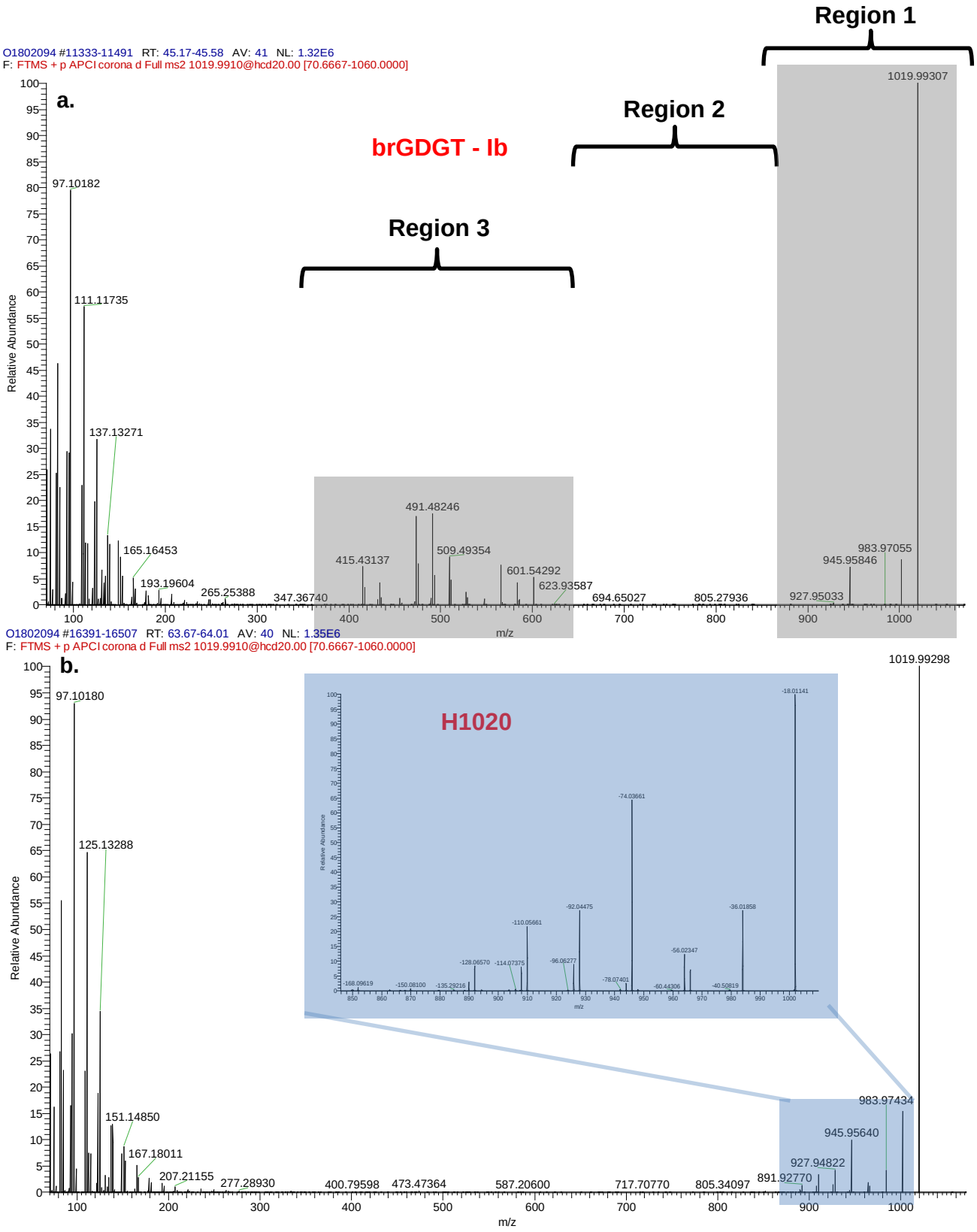

Figure 16. MS^2 spectra showing the fragmentation patterns of the (a) regular brGDGT with m/z of 1020, with fragmentation in regions 1 and 3 and (b) the H-brGDGT H1020 which has the particular framgmentation pattern expected from and H-shaped GDGT, with fragmentation occuring only in region 1. The distinction of regions is taken from Knappy et al. (2009; 2015).

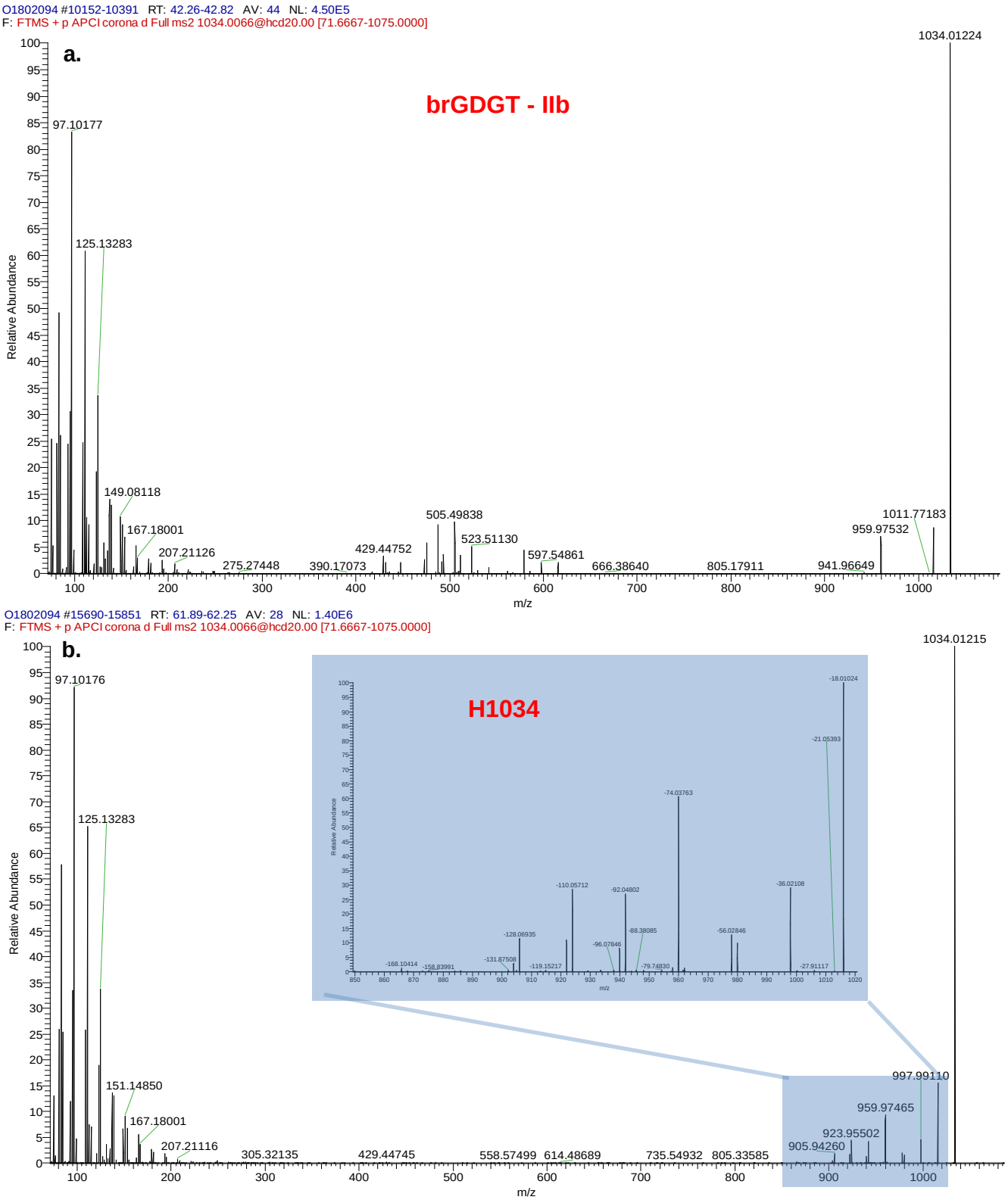

Figure 17. MS^2 spectra showing the fragmentation patterns of the (a) regular brGDGT with m/z of 1034, with fragmentation in regions 1 and 3 and (b) the H-brGDGT H1034 which has the particular framgmentation pattern expected from and H-shaped GDGT, with fragmentation occuring only in region 1. The distinction of regions is taken from Knappy et al. (2009; 2015).

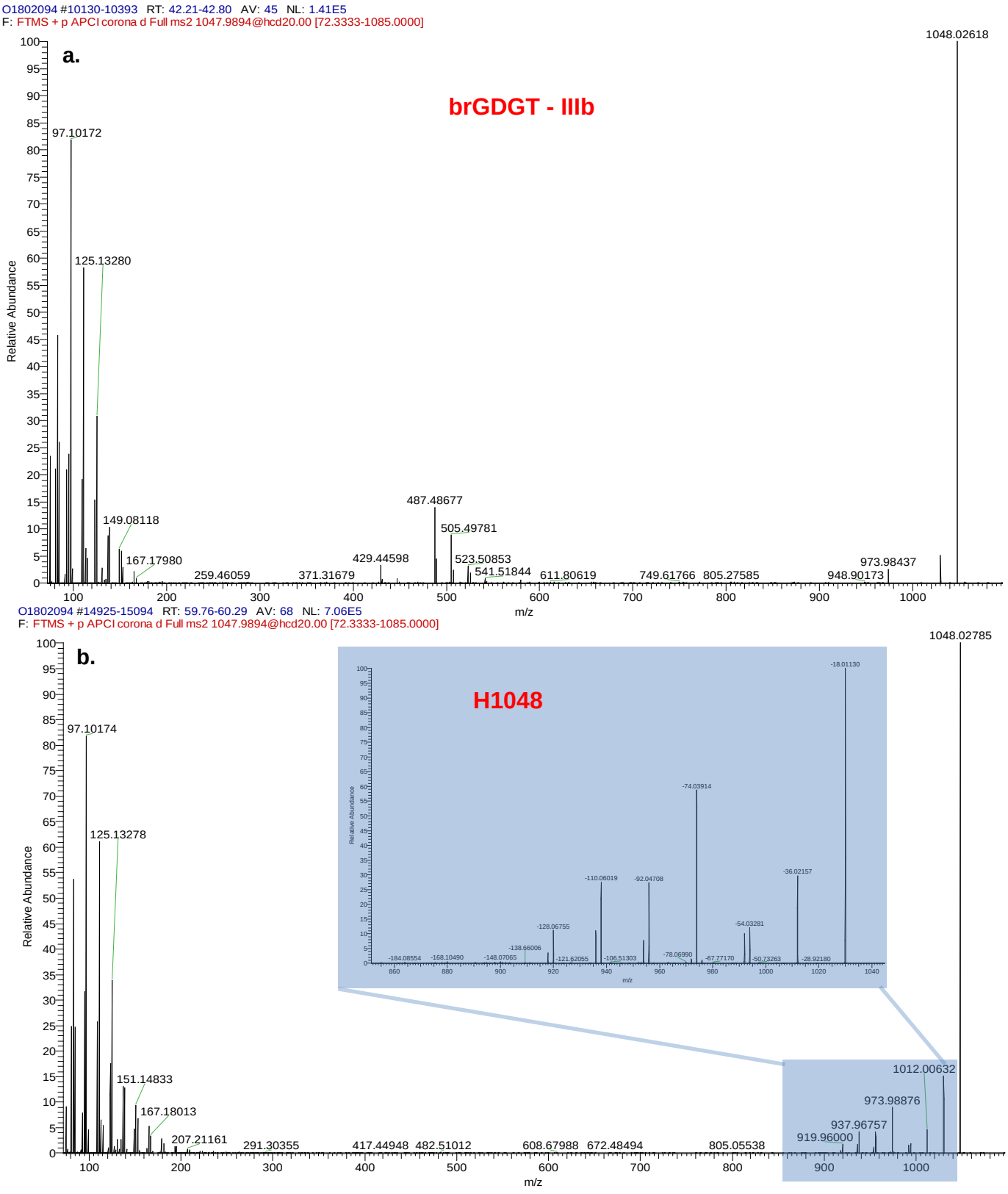

Figure 18. MS^2 spectra showing the fragmentation patterns of the (a) regular brGDGT with m/z of 1048, with fragmentation in regions 1 and 3 and (b) the H-brGDGT H1048 which has the particular framgmentation pattern expected from and H-shaped GDGT, with fragmentation occuring only in region 1. The distinction of regions is taken from Knappy et al. (2009; 2015).

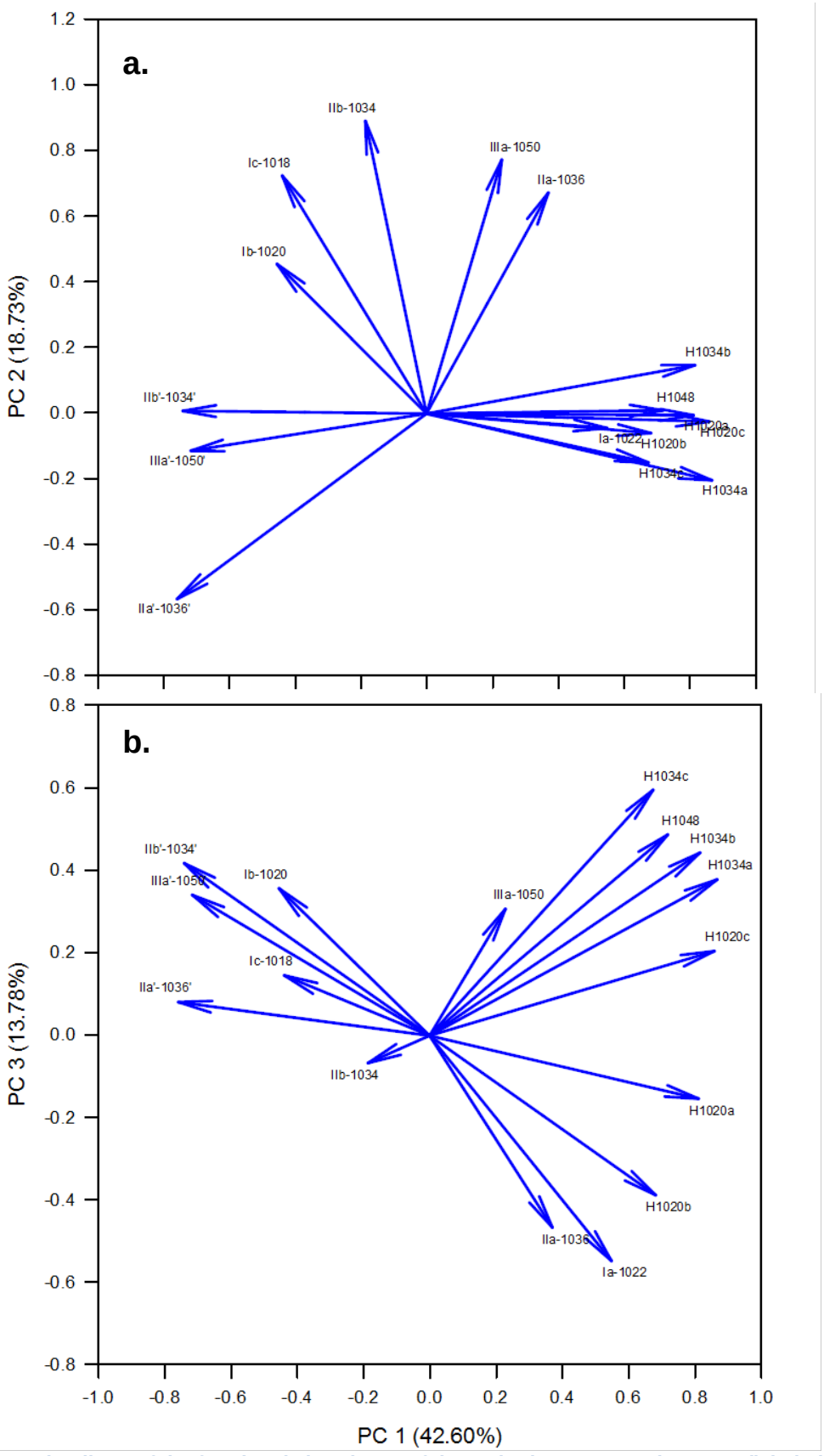

Figure 19: PCA loadings of the fractional abundance of the major brGDGTs and GMGTs (labeled H) from the Lake Challa samples.

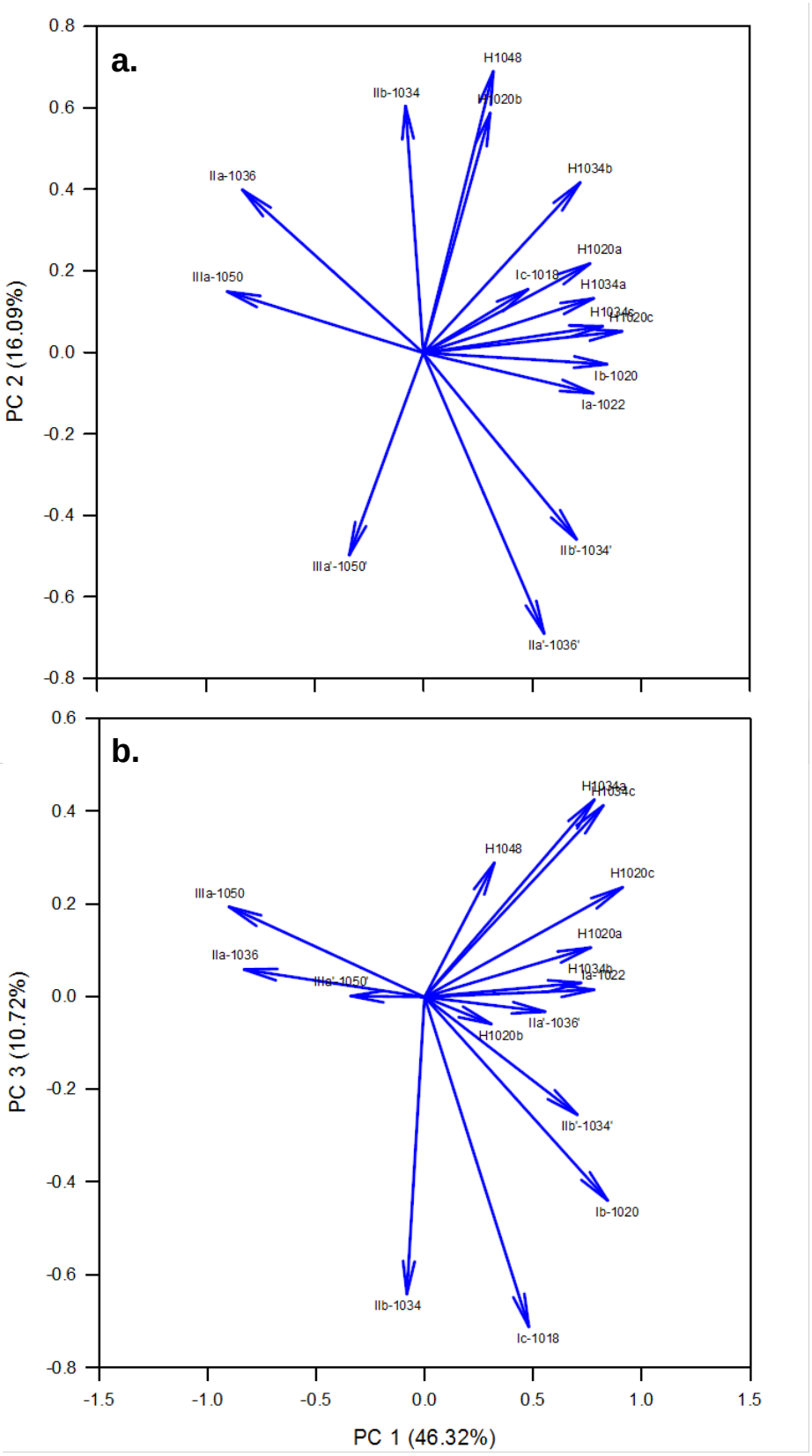

Figure 20: PCA loadings of the fractional abundance of the major brGDGTs and GMGTs (labeled H) from a set of East African lake sediments (Russel et al. 2018)

of variable BIT values lasting around ten thousand years, suggesting a generally wetter and variable climate during this interval

From 140 to 70 ka, the BIT record of Lake Challa displays a greater magnitude of changes than shown in the most recent 25 kyrs (Verschuren et al. 2009). Whereas the BIT record from 25 to 0 ka reaches a minimum of 0.3, during the LMG and Younger Dryas (Fig. 11), the BIT record presented here remains below 0.2 for most of the time series. The BIT proxy therefore appears to also indicate the severity and not just the timing of dry periods. In this way, the BIT proxy is not only a threshold indicator of severe rainfall events (Buckles et al. 2016) but can provide insights into the degree of aridity in the past.

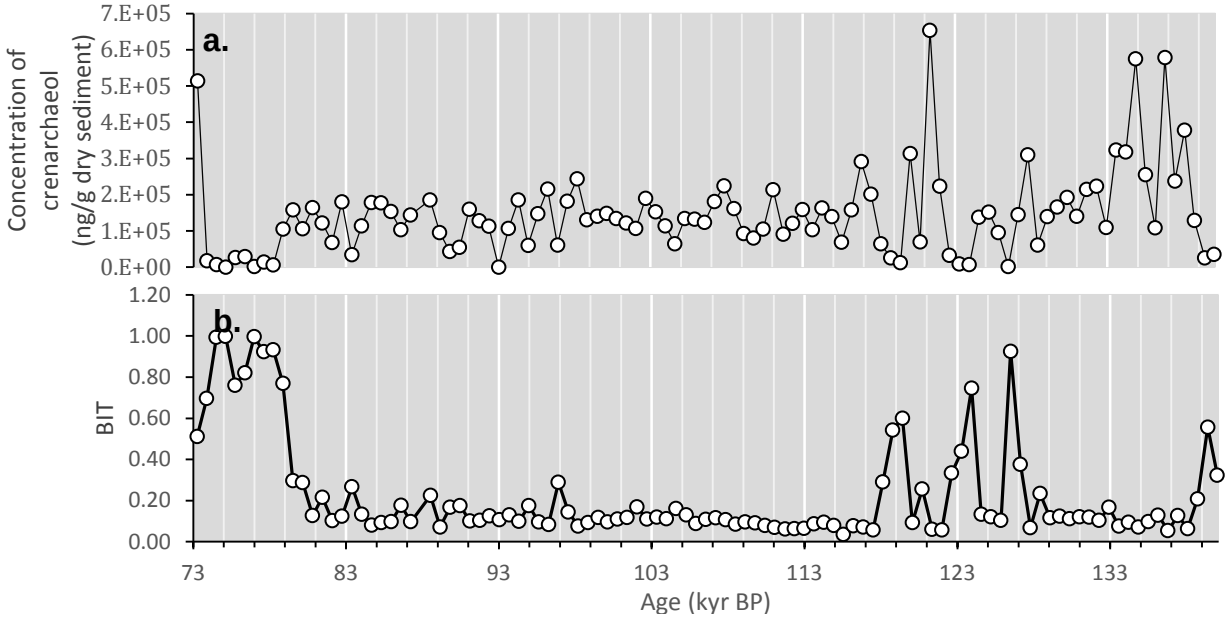

Figure 21. Plot (a) shows the concentration of crenarchaeol over time, calculated according to Equation 13 and plot (b) shows the BIT index for Lake Challa.

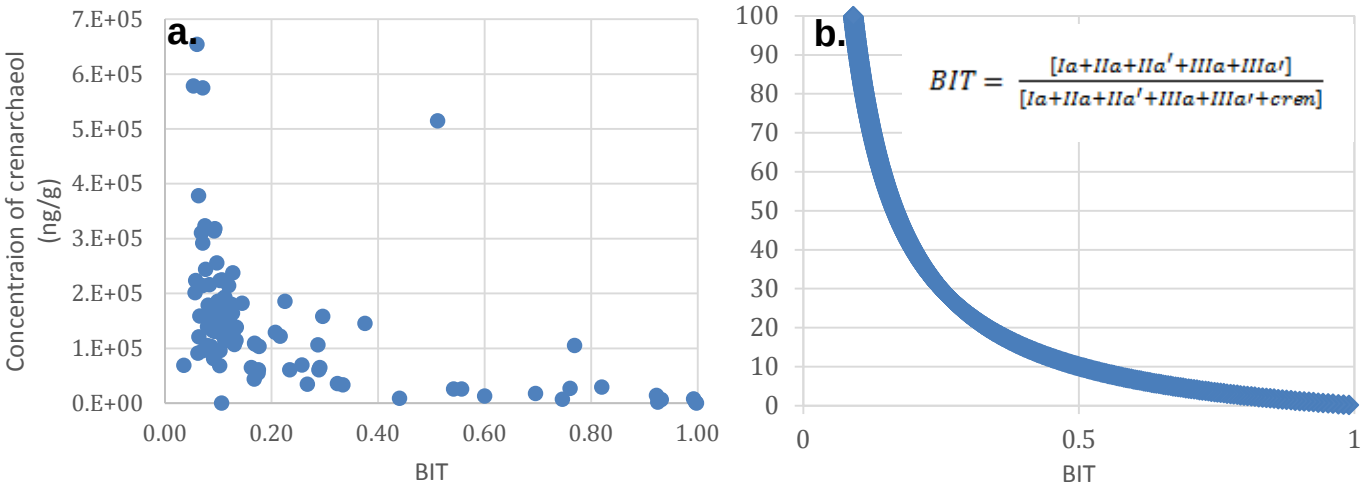

Figure 22. Plot (a) shows BIT versus the concentration of crenarchaeol of the Lake Challa samples. Plot (b) shows the relationship between BIT and concentration of crenarchaeol where the abundance of brGDGTs is constant and changes in the BIT index are controlled entirely by changes in crenarchaeol.

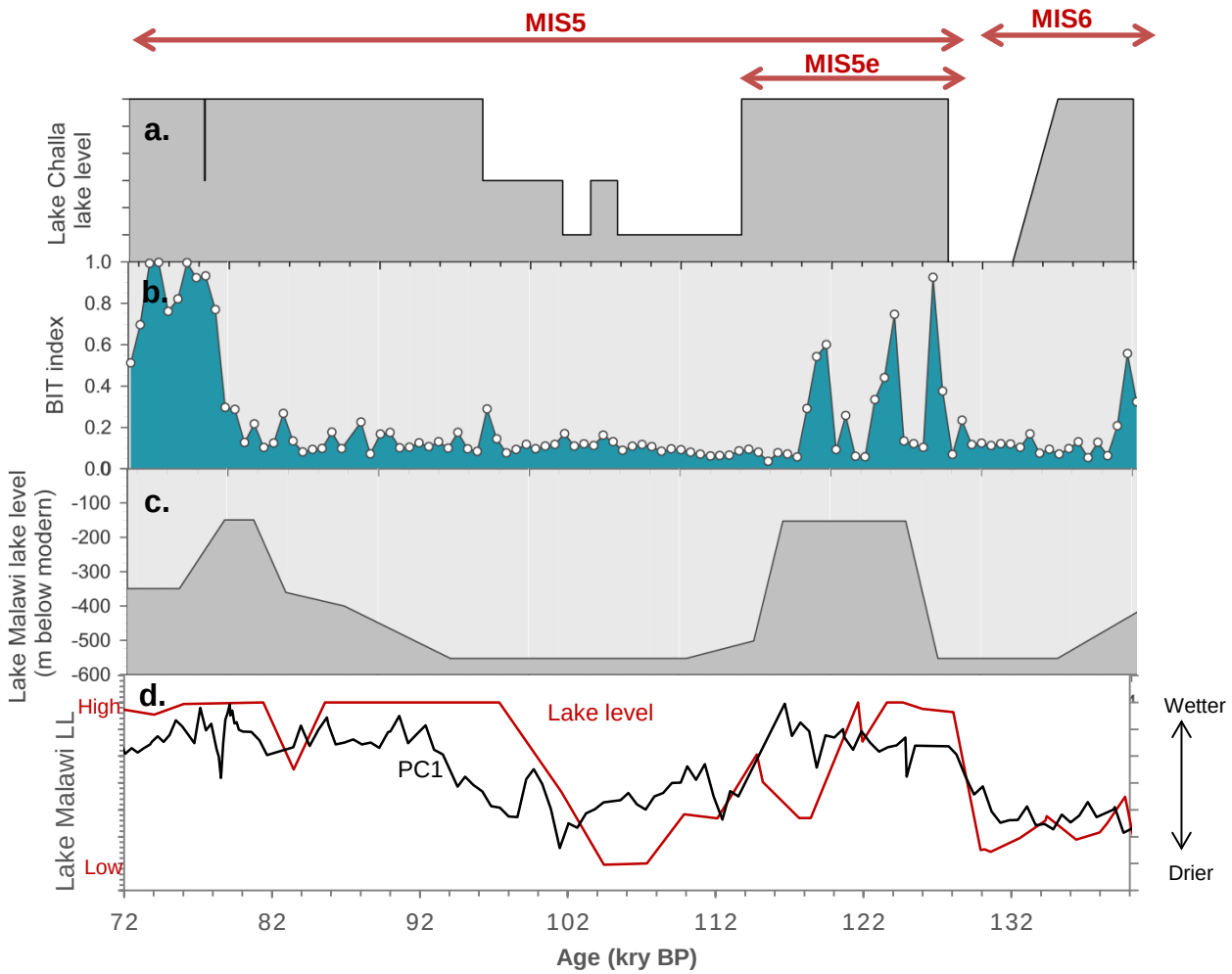

Figure 23. (a) The lake level record for Lake Challa based on seismic reflection data (Moernaut et al 2010), (b) the Lake Challa BIT index presented in this study and (c) the Lake Malawi lake level record based on seismic reflection data (Scholz et al. 2007) using the old age model. (d) The red line in plot the lake level record of Lake Malawi using the revised age model (Johnson et al. 2016 and the black line is the PCI axis of Lyons et al. 2015) summarizing the precipitation proxies from Lake Malawi. It illustrates changes between wet and dry conditions.

Previous research found that variations in the BIT record over the last 2200 years at Lake Challa had a strong negative correlation with fluctuations in the concentration of crenarchaeol (Buckles et al. 2016). Buckles et al. (2016) explained that the introduction of nutrients into the lake system by runoff indirectly leads to the suppression of *Thaumarchaeota* during rainy intervals, thus causing rainy periods to be associated with higher BIT values. During the time series presented here, the absolute concentration of crenarchaeol in Lake Challa also fluctuates (Fig. 21a; Appendix 1), and shows a negative correlation with the BIT index (Fig. 22a). Several of the samples with the lowest crenarchaeol concentrations correspond to peaks in the BIT index (Fig. 21a,b). For example, this is especially clear in the interval after 80 ka, where BIT values increase dramatically, and the lowest concentrations of crenarchaeol occur. The plot presented in Figure 22b is the expected relationship between the BIT index and the concentration of crenarchaeol when the concentration of the brGDGTs remains constant and only the concentration of crenarchaeol is influencing the BIT values. This expected correlation is similar to the relationship between BIT and the concentration of crenarchaeol observed in Lake Challa (22a). Therefore, as put forth by Buckles et al. (2016), the BIT index is correlated to rainfall history at Lake Challa through fluctuations of crenarchaeol.

As was observed for the first 25 kyrs at Lake Challa, there is a general agreement between the BIT record and the seismic lake level record for this period. Particularly, the timing of the wetter period separating the two megadroughts corresponds well with a recorded highstand in Lake Challa and also to the timing of MIS5e, the anticipated warmest part of the last interglacial (Fig. 23). At first it would appear that there is a divergence between rainfall and lake level, presented in the BIT and seismic records respectfully, in regards to the timing of the return to wetter conditions after the second recorded megadrought. In the seismic record, lake level rises around 102 ka whereas the BIT index only shows a return to rainy conditions after 80 ka. However, the lake level record is based on the interpretation of certain sedimentological features, such as erosional features and draped sedimentation, as indicating high and lowstands in the lake's history. Some of these features can appear at a range of depths and therefore the magnitude of the lake-level changes in Lake Challa cannot be determined precisely by this method, whereas the timing of the events can be more accurately established. Thus it is possible that lake level after to 80 ka was indeed much higher than prior to 80 ka.

The lake level of Lake Challa is controlled by local rainfall, run-off, evaporation, and groundwater inflow and outflow. As mentioned, sub-surface inflow represents a major part of the hydrological budget of Lake Challa, and likely also did in the past. It may also then be possible, that the difference in the length of the second megadrought could reflect a disconnect between lake level and amount of local rainfall, and that for this period of offset Lake Challa was fed dominantly by groundwater inflow. The Lake Challa BIT record presented here shows a striking resemblance to the lake level history of Lake Malawi (Fig 23c) presented by Scholz et al. (2007) based on the original age prior to the discovery of the YYT. The Lake Malawi seismic record suggests a return to wetter conditions began around 94 ka and that level was again high at 82 ka (Scholz et al 2007). Lake Malawi, which currently lies within the southern reaches of the ITCZ, is a hydrologically open lake, meaning that it is fed mostly by rainfall.

The revision of the Lake Malawi chronology led to a shift in the timing of the megadroughts (Lane et al. 2013). Using the new age model, proxy precipitation data also shows the occurrence of megadrought during MIS5 but which lasted a much shorter interval than presented by Scholz et al. (2007; Fig. 23d, black line). The lake level record (Fig 23d, red line), wet conditions return to Lake Malawi by ca. 98 ka following the MIS5 megadrought. A further independent measure for lake level or watershed moisture availability also exists for Lake Malawi based on the assemblages of fossils preserved in the lake sediments (Lyons et al. 2015). The variance of the fossil assemblages controlled by moisture availability is summarized by the PC1 axis (Fig. 23d, black line). PC1 versus Age for Lake Malawi represents changes between wet and dry conditions, and shows a complicated history of moisture variability, but also details periods of increased aridity. In the PC1 plot, moist conditions return just after 100 ka, and generally persist until present. Given the uncertainty involved in the Lake Malawi chronology over the MIS5 and MIS6 periods it is difficult to draw direct comparisons. The BIT index of Lake Challa given here certainly presents the most striking evidence for prolonged and severe megadroughts during this interval compared to the other precipitation proxies for Eastern Africa which are currently available.

As discussed above in section 1.3.2, the appearance of coincident droughts in lakes Malawi and Challa is somewhat puzzling. During periods of extreme insolation variability, there is intensification of the Asian monsoon, which in turn causes the average position of the ITCZ may shift northward (Blome et al. 2012). Regions at the southernmost limits of the African tropics, like Malawi, will be greatly affected by this change and experience drought conditions. However, Lake Challa positioned close to the equator will not be impacted in the same way. Assuming the Scholz et al. (2007) chronology is correct, the accordance of the Challa BIT record with the Lake Malawi lake level record would imply that the amplified precessional cycle during MIS5 by itself cannot explain this megadrought, certainly not at Lake Challa.

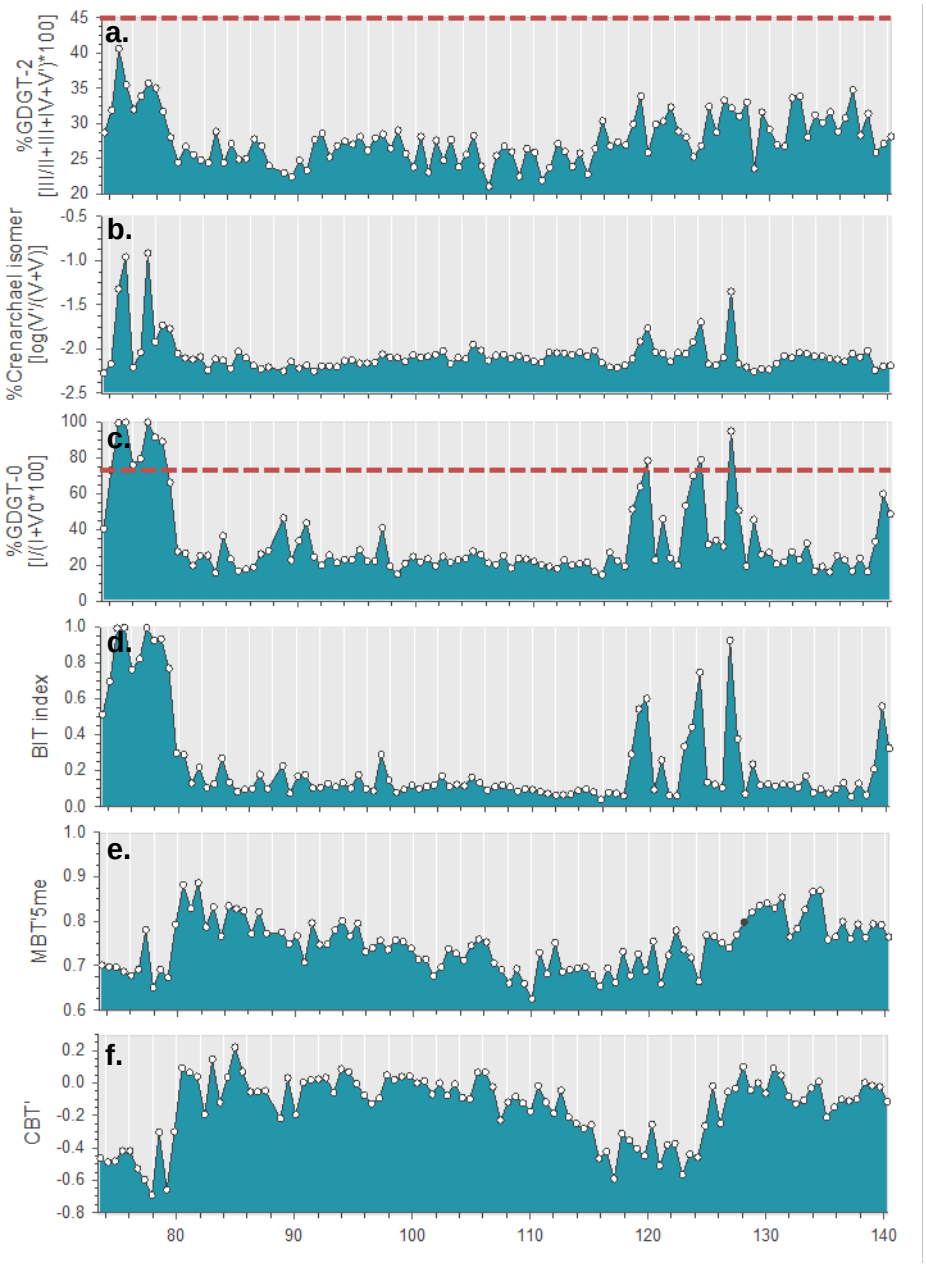

Figure 24. Ratios of iso and brGDGTs from Lake Challa.

4.1.2 TEX_{86} based palaeotemperature reconstruction

Before calibrating the results of the application of TEX_{86} index to lake surface temperature (LST) it is advisable to filter out data points for which the application of TEX_{86} may not provide an accurate estimate of temperature, this is mainly due to the possibility of other sources for the isoGDGTs other than the nitrifying archaea *Thaumarchaeota* living in the upper water column. Following the method of Sinninghe Damsté et al. (2012a), which was used when evaluating past temperature changes durinig the last 25,000 years at Lake Challa, we can determine whether TEX_{86} should be applied. Firstly, the data is checked for the potential contribution of isoGDGTs by methanogenic archaea. Methanogenic archaea produce relatively more GDGT-0 than pelagic *Thaumarchaeota*, which normally produce GDGT-0 to crenarchaeol at a ratio of less than 2 (Blaga et al. 2009). When %GDGT-0 (defined as the contribution of GDGT-0 to the sum of GDGT-0 and crenarchaeol) exceeds 67% this implies a substantial contribution of methanogens to the isoGDGTs and therefore these data points must be excluded from the time series. The plot of %GDGT-0 covering the last interglacial period occasionally exceeds 67% (demarcated by the red line in Fig. 24c) and exclusively during periods of high rainfall, as shown by the results of the BIT index, during the periods 128-118 ka and after 80 ka.

Secondly, in marine surface sediments, the %GDGT-2 ranges from 20-45%, whereas in modern Lake Challa surface sediments this value is substantially higher (ca. 55%; Sinninghe Damsté et al. 2012). It is therefore possible that when %GDGT-2 exceeds 45%, GDGT-2 may be originating from other sources than pelagic *Thaumarchaeota* and may lead to an overestimation of temperature. In the section of the core presented here, however, the %GDGT-2 does not exceed 45% (Fig. 24a).

The similarity between the %GDGT-0 and the BIT index versus age plots is likely due to the fluctuation of crenarchaeol in the lake, as both ratios are defined relative to crenarchaeol. This is also somewhat visible in the plot of %crenarchaeol isomer (also calculated as the relative contribution of the regioisomer to the sum of the isomer and crenarchaeol (Fig. 24b); note the logarithmic scale). Sinninghe Damsté et al. (2012) attributed the positive correlation between the BIT index, %GDGT-0 and %crenarchaeol isomer which they observed in the 25 ka record of Lake Challa, as the result of the inclusion of soil derived *Thaumarchaeota*, which produced the crenarchaeol regioisomer in at a higher relative abundance to crenarchaeol than aquatic *Thaumarchaeota*.

After excluding the samples where %GDGT-0 was above 67%, three different TEX86 – LST calibrations were applied to the data: those of Tierney et al. (2010a), Powers et al. (2010) and Castañeda and Schouten (2011; Note that corrections of these calibrations were published by Castañeda and Schouten (2015) and that the plots presented here are based on the revised calibrations). The calibrations of Powers et al. (2010) and Castaneda and Schouten (2011) estimated temperatures between 8°C and 15°C, and the calibration of Tierney et al. (2010a) provided a temperature reconstruction of a few degrees higher, between 12°C and 17°C (Fig. 25b). All three calibrations yielded temperatures which are much lower than expected for Lake Challa during this period.

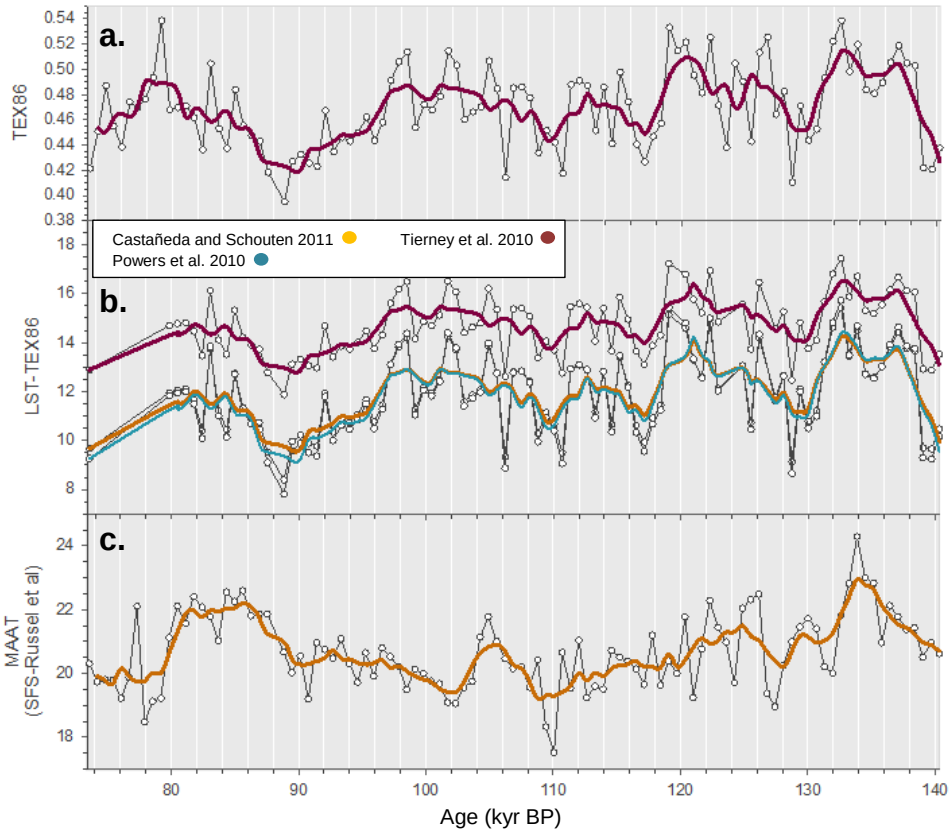

Figure 25. Plot (a) is the raw unfiltered TEX_{86} values and plot (b) shows the temperature estimation after the filtering of data points according to the methods mentioned in text and application of the calibrations of Tierney et al. (2010; purple line), Powers et al (2010; blue line) and Castaneda and Schouten (2011) as corrected in Castaneda and Schouten (2015). Plot (c) shows the temperature estimation using the method of Russel et al. (2018) based on the distribution of brGDGTs (Equation 10). In all the plots individual data points are plotted as open circles and the solid coloured lines are the 5-point moving average of the data points.

The relative abundance of crenarchaeol appears to be atypically low for a tropical lake in some of the Lake Challa samples and the large changes in crenarchaeol recorded down core are likely too extreme to be related to temperature fluctuations alone. Although crenarchaeol itself is not used to calculate TEX_{86}, *Thaumarchaeota* also produce significant amounts of the lesser isoGDGTS. Therefore, when the relative abundance of crenarchaeol is very low, this may suggest that *Thaumarchaeota* may not be prolific enough to be the major influencer on the TEX_{86} signal. It is possible that the use of TEX_{86} may not be appropriate at Lake Challa because of the unique behaviour of *Thaumarchaeota* in relation to rainfall, which produce isoGDGTs used in the TEX_{86} formula.

4.1.3 brGDGTs based palaeotemperature reconstruction

The distribution of brGDGTs was also used to reconstruct paleotemperature over this interval. Using the SFS calibration of Russel et al. (2018; Equation 10), the distribution of certain brGDGTs were related to MAAT, result in temperatures ranging from 18°C to 24°C (Fig. 25c). The highest temperatures were reached around 135 ka, after which they decrease generally until 108 ka. Temperatures peak slightly around 105 ka, after which they increase more

gradually towards relatively high temperatures (ca 22°C) during the period 88-80 ka. After 80 ka, temperatures are generally a few degrees lower.

Due to the abnormally low temperatures predicted by TEX_{86} and the unique behaviour of *Thaumarchaeota* in Lake Challa, the reconstruction of MAAT based on brGDGTs appears to be a more reliable estimate of past temperature changes in Eastern Equatorial Africa. Although the Lake Challa record shows that the highest temperatures occurred several thousand years before the warmest interval of the interglacial, MIS5e, there is similarity between the general trend of the MAAT record from Lake Challa and the Vostok δD record (Fig. 26) and several key features of the ice age record also seem to appear in the Lake Challa temperature record (red arrows in Fig. 26). Further, as the age model for the DeepCHALLA core is not yet fully established, it is possible that the Lake Challa time series may shift slightly.

Beside ice sheet records it is also likely that temperature variability at Lake Challa shows similarities to other sites in East Africa or in the Indian Ocean. However, due to the preliminary nature of the Lake Challa age model and the low resolution of some proxy records during this time interval, it is difficult to draw comparisons. For example, it is difficult to see striking similarities between temperature variability at Lake Challa and SST fluctuations in the Indian Ocean (based on Mg/Ca) or the Gulf of Aden (based on alkenones), or paleotemperature of Lake Malawi (based on TEX_{86}) during this period (Fig. 27).

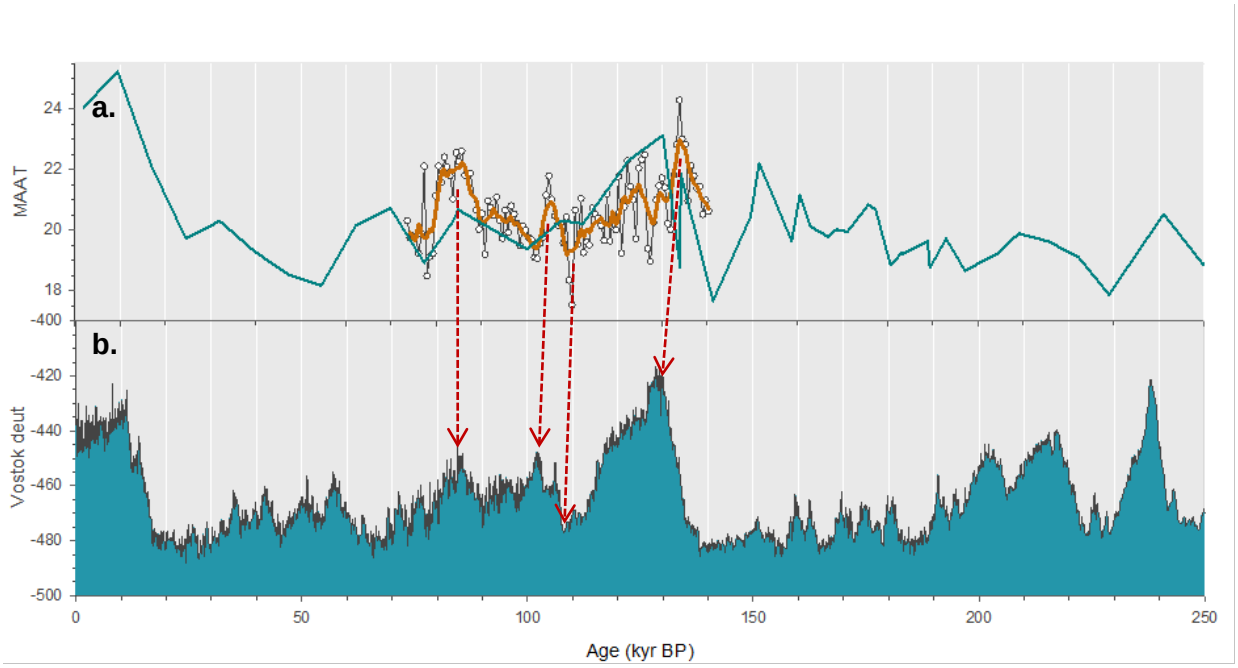

Figure 26. In plot (a) the blue line represents the unpublished results from a test study by Sinninghe Damsté and Verschuren which shows a temperature reconstruction for the last 250,000 years based on the distribution of brGDGTs in Lake Challa (Eq. 10; Russel et al 2018). In plot (a) the open circles are the data points from this study, which also use the distribution of brGDGTs to estimate temperature, from the period 140 – 70 ka. The orange line is a 5 point running average of the results from this study. Plot (b) is a graph of the deuterium record from the Vostok core, Antarctica (Lorius et al. 1995).

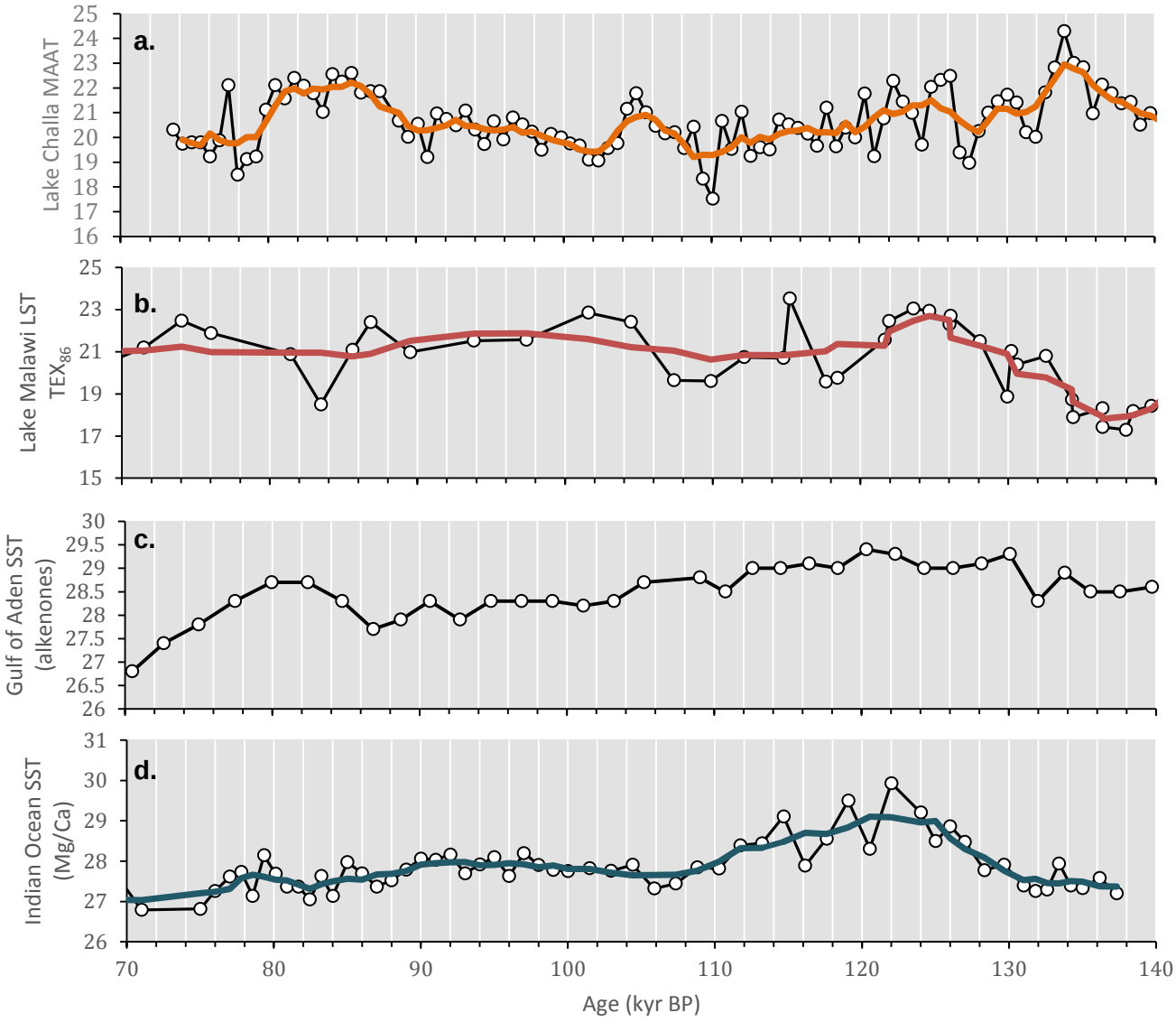

Figure 27. (a) The paleotemperature reconstruction for Lake Challa presented in this report based on the distribution of brGDGTs. (b) Lake Malawi lake surface temperature reconstructed using TEX_{86}-LST calibration (Powers et al. 2010). (c) Alkenone bases SST reconstruction for the Gulf of Aden (Tierney et al. 2017). (d) Indian Ocean SST reconstruction using Mg/Ca (Saraswat et al. 2005). Open circles are individual data points and solid lines are the 5 point moving average of the data points.

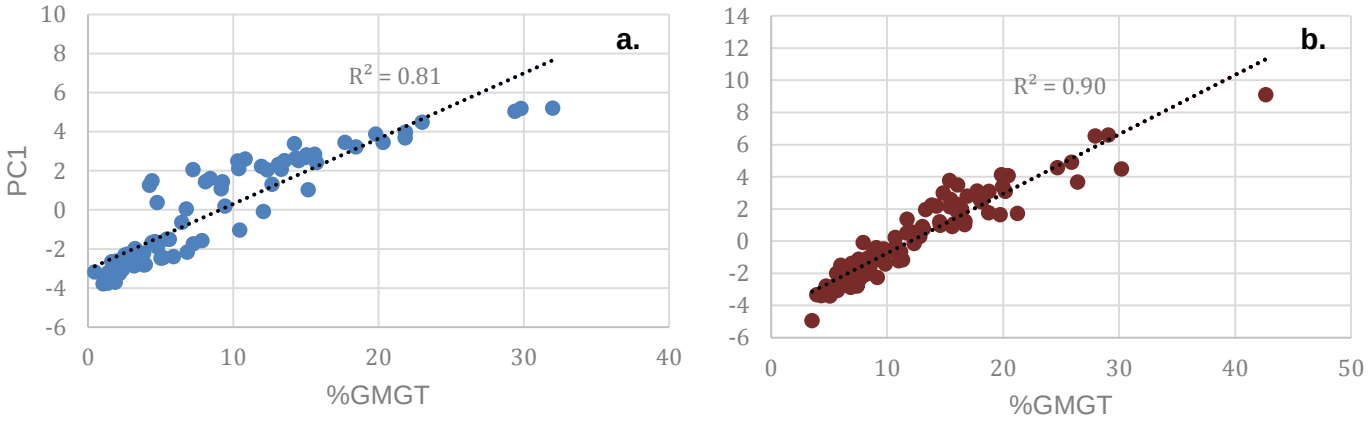

Figure 28. (a) Plot %GMGT (calculated as the contribution of all the brGMGT isomers to the sum of the brGMGTs and brGDGTs) versus the PC1 scores for the East African lake set (Russel et al. 2018) and (b) for the Lake Challa samples analysed as part of this study.

4.2 GMGTs as potential proxies

4.2.1 Distribution and potential sources of brGMGTs

Branched and isoprenoid GMGTs have been found in sediments dating to the Jurassic (Bauersachs and Schwark 2016), revealing that these compounds are preserved on geological timescales. In total, six isoGMGTs and three brGMGTs have been identified (Knappy et al. 2009; 2011; 2015; Naafs et al. 2018, Liu et al. 2012, Jaeschke et al. 2012; Bauersachs and Schwark 2016). Significantly, this adaptation is seen in both the archaea and bacteria domains, possibly suggesting the last common ancestor had this trait (Naafs et al. 2018).

Several inferences can be made from the PCA of the Lake Challa and East African Lake brGMGTs about the controls and sources of the brGMGTs. Firstly, it is possibly that the brGMGTs are produced by the same source organism as they are closely grouped in the PCA loadings plots. Unlike the 5me- and 6me-brGDGTs, the isomers of the brGMGTs do not plot separately from one another. In the PCA plot of Lake Challa, brGDGT-Ia plots within this cluster and may therefore be produced by the same source organism. It also appears that the brGMGTs often plot with the acyclic brGDGTS, supporting that they represent acyclic lipids, and could also possibly suggest that the organisms which produce brGMGTs cannot synthesize rings or that the stereochemistry of the lipid is such that the inclusion of the carbon-carbon bond prevents the formation of rings (Naafs et al. 2018). This fits with the findings from Lake Challa, where no cyclic brGMGTs were identified in the sedimentary record. The brGMGTs also often group with the 5me-brGDGTs, and plot very differently in the PCA loading plots than the 6me-brGDGTs, suggesting that the branching of the brGMGTs may also occur at the 5 methyl position.

4.2.2 Potential for use of GMGTs as paleotemperature indicator

Although it has been suggested that the ‘H-bond’ enhances membrane stability at higher temperatures (Morri et al. 1998; Schouten et al. 2008), only more recently has the purpose of this adaptation been compellingly explained (Naafs et al. 2018). In a global peat data set from 96 different peatlands the brGMGTs m/z 1020, 1034 and 1048 were identified and the relationship

between temperature and relative abundance of brGMGTs was investigated. They do, however, not report on the abundance of different isomers of the brGMGTs. The study found a positively correlation between temperature and the relative abundance of brGMGTs but with significant scatter, indicating that other factors also likely contribute to the relative abundance of GMGTs. The highest relative abundance of GMGTs occurred in tropical peatlands, with the highest relative abundance of isoGMGTs recorded in Peru at 11%, and of brGMGTs in Indonesia at 26%. Naafs and colleagues (2018) redefined the MBT index to include only the acyclic brGDGTs ($MBT_{acyclic}$; Eq. 17) and compared this to the methylation of the brGMGTs summarized in the new H-$MBT_{acyclic}$ index (Eq. 18).

$$MBT_{acyclic} = \frac{brGDGT-Ia}{[brGDGT-Ia + brGDGT-IIa + brGDGT-IIa' + brGDGT-IIIa + brGDGT-IIIa']} \quad (17)$$

$$H\text{-}MBT_{acyclic} = \frac{brGMGT-Ia}{[brGMGT-Ia + brGMGT-IIa + brGMGT-IIIa]} \quad (18)$$

In Equation 18 above, brGMGT-Ia, brGMGT-IIa and brGMGT-IIIa refer to brGMGTs H1020, H1034 and H1048 respectively. In the peat data set it appeared that the degree of methylation of the brGDGTs was linearly correlated with the methylation of brGMGTs. Thus, Naafs et al. (2018) proposed that brGMGTs are possible produced by the same organisms as brGDGTs. The H-$MBT_{acyclic}$ can also be rewritten to include the additional brGMGT isomers which are present in the Lake Challa sediments and many of the East African lakes, but are not reported in the peat data set:

$$H\text{-}MBT'_{acyclic} = \frac{[H1020a+H1020b+H1020c]}{[H1020a+ H1020b+H1020c+H1034a+H1034b+H1034c+H1048]} \quad (19)$$

For Lake Challa there is also a positive correlation between $MBT_{acyclic}$ and H-$MBT'_{acyclic}$ (R^2=0.45; Fig. 29b). In contrast, for the East African lake data set no correlation between H-$MBT'_{acyclic}$ and $MBT_{acyclic}$ exists (Fig 29a).

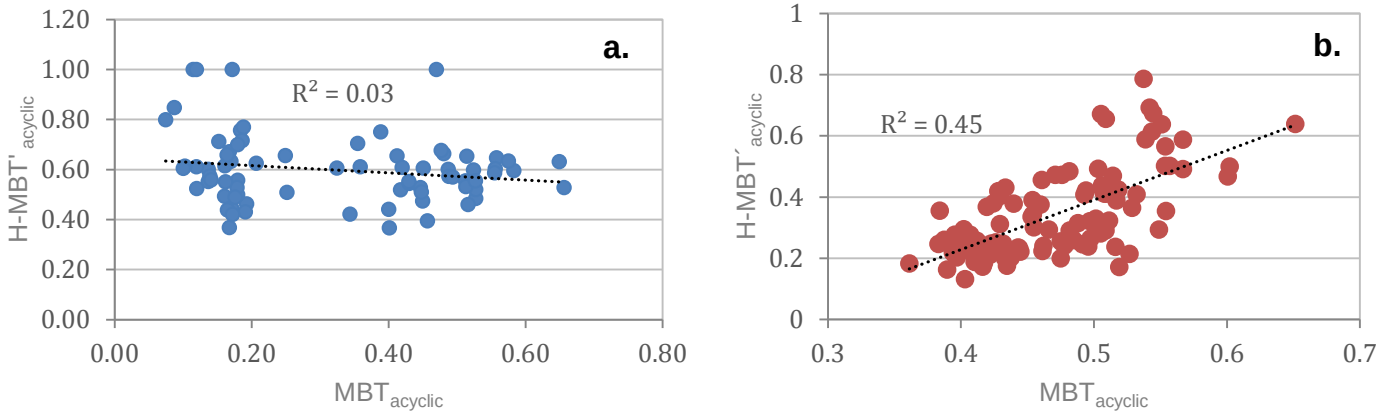

Figure 29. H-$MBT'_{acyclic}$ versus $MBT_{acyclic}$ for (a) the East African Lake Data set and (b) the Lake Challa samples.

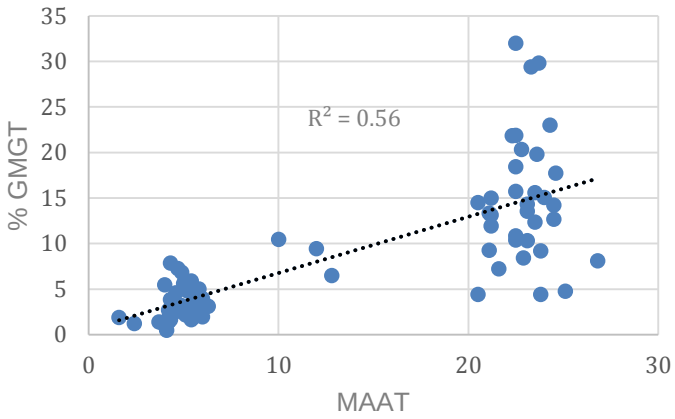

Figure 30: %GMGT (defined as the relative contribution of all brGMGT isomers to the sum of all regular and H-shaped brGDGTS) versus measured MAAT from East African Lakes.

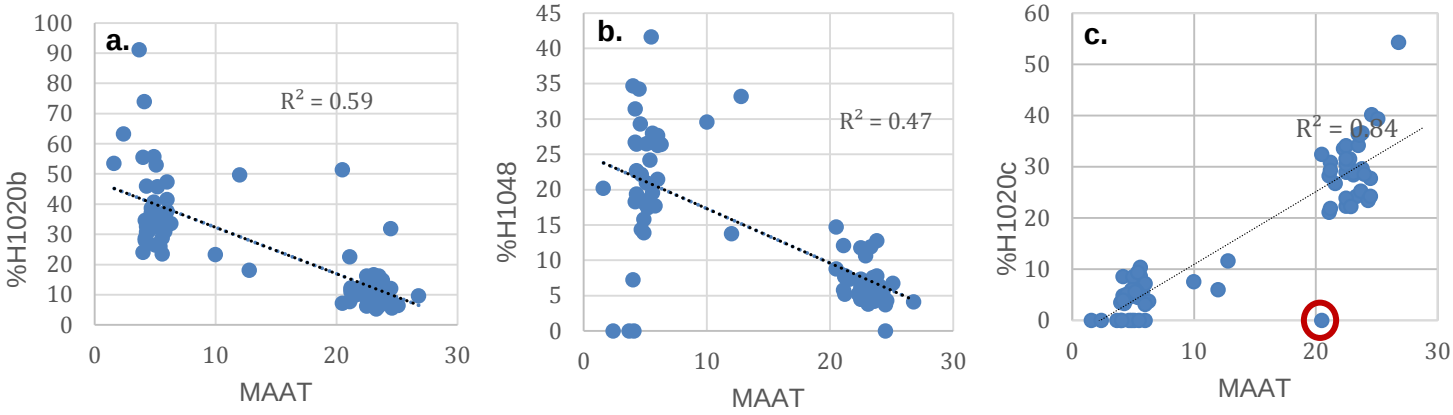

Figure 31. Relative abundance of brGMGT isomers calculated as the contribution of the individual isomer to the sum of all the brGMGTs.

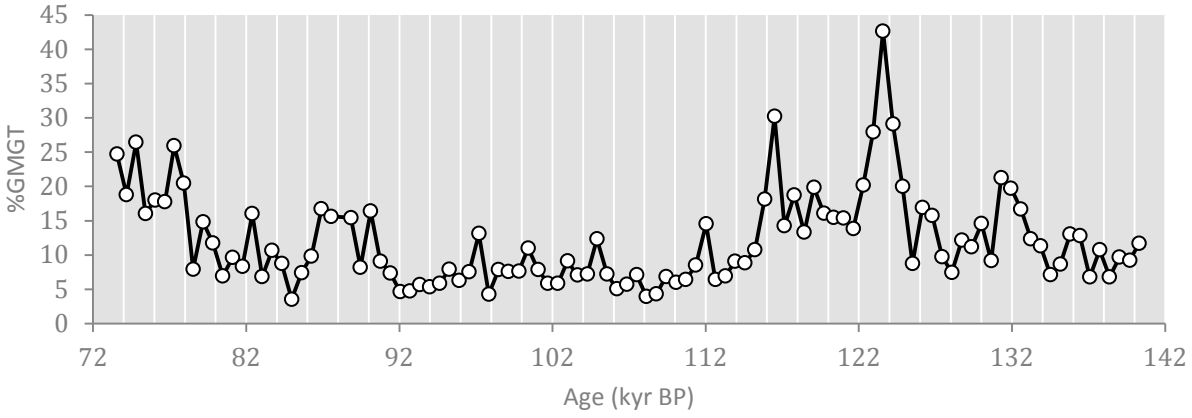

Figure 32. Plot of the %GMGT (defined as the relative contribution of all the brGMGT isomers to the sum of the brGMGTs and the brGDGTs over time in the Lake Challa core.

Using the distributions of the East African Lake Data set, we can observe if the brGMGTs display a relationship to temperature. Generally, the %GMGT was higher in East African lakes with higher measured MAAT. The highest %GMGT was 32% from Lake Murusi, Uganda, which has a MAAT of 22.5°C. In the graph of %GMGT versus MAAT there is, however, substantial scatter for lakes with a MAAT above 20°C (Fig. 30). This is also true when plotting the fractional abundance of most of individual brGMGT isomers (defined as the contribution of the individual isomers to the sum of all brGMGT isomers) against MAAT. In order to create ratios between isomers which will have a strong correlation to MAAT, isomers with the least scatter when plotted against MAAT, especially at temperatures above 20°C, were selected. In Fig. 31, the fractional abundances of isomers H1020b, H1020c and H1048 are plotted against MAAT. There is a relative increase in %H1020c and decrease in %H1020b and %H1048 with increasing MAAT. Ratio 1 (Eq. 20) captures this relationship, showing that at higher temperatures isomer H1020c has a higher contribution to the sum of H1020b and H1020c. Ratio 1 has a significant correlation to MAAT (R^2=0.86; Fig. 33). This correlation is slightly increased (R^2=0.92) with the exclusion of the outlier data point circled in red and also present in the plot of %1020c versus MAAT (Fig. 31c). Ratio 2 (Eq. 22), is based on the observation that at higher temperatures the relative contribution of H1020c to the sum of H1020c and H1048 increases. Ratio 2 also has a significant correlation to MAAT (R^2 = 0.88; Fig. 34), and this correlation is improved by exclusion of the outlier (R^2=0.94).

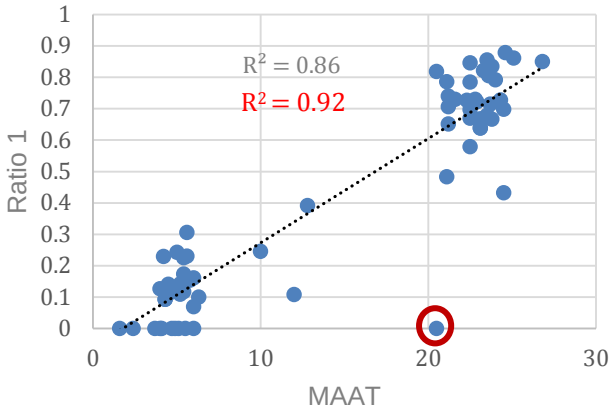

$$\text{Ratio 1} = \frac{[\text{H1020c}]}{[\text{H1020b+H1020c}]} \quad (20)$$

$$\text{MAAT} = 29.5*(\text{Ratio1}) + 1.78 \quad (21)$$

Figure 33. East African Lake set data. Ratio 1 is defined as the relative contribution of H1020c to the sum of H1020b and H1020c and is shown plotted against MAAT.

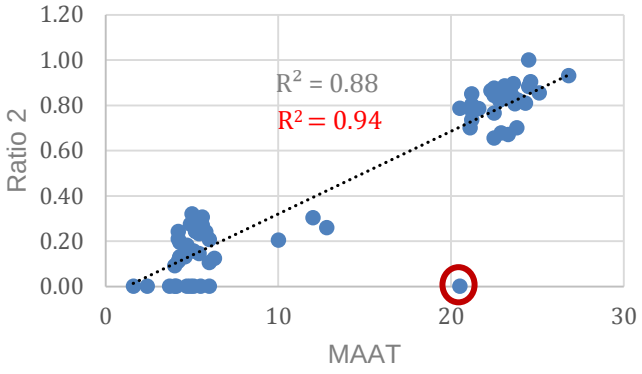

$$\text{Ratio 2} = \frac{[H1020c]}{[H1048+H1020c]} \quad (22)$$

$$\text{MAAT} = 26.74*(\text{Ratio2}) + 1.25 \quad (23)$$

*Equations 21 and 23 above were calculated excluding the single outlier point circled in red.

Figure 34. East African Lake set data. Ratio 1 is defined as the relative contribution of H1048 to the sum of H1020b and H1048 and is shown plotted against MAAT.

It is clear from the brGMGT distributions of the East African Lakes that generally more isomers of H1020 and H1034 appear at higher temperatures, whereas at lower temperatures commonly only the H1020b and H1034b isomers are present (Fig. 15). In Lake Challa for example, all H1020 and H1034 isomers are present in each sample, although their relative abundance to one another is not consistent. To assess the relationship between the distribution of the H1020 and H1034 isomers and temperature a new isomerization ratio for the brGMGTs (IR_{brGMGT}) can be defined as shown in Equation 24. The IR_{brGMGT} of the East African Lake sediments has a strong correlation to MAAT (R^2=0.82, Fig. 35), and much less scatter at higher temperatures than seen in the plot of %GMGT to MAAT.

$$IR_{brGMGT} = \frac{[H1020b+H1034b]}{[H1020a+H1020b+H1020c+H1034a+H1034b+H1034c]} \quad (24)$$

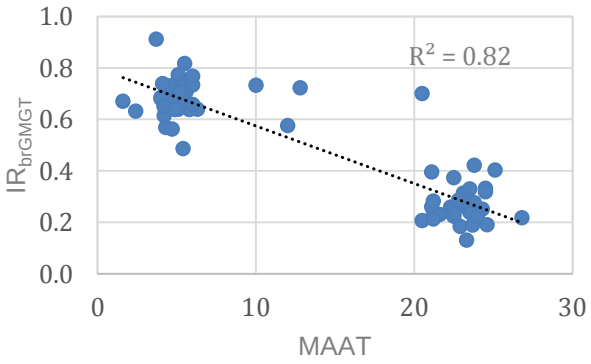

$$MAAT = -44.64*(IR_{brGMGT})+35.652 \quad (25)$$

Figure 35. East African Lake data. Isomerization ratio of brGMGTs (Eq. 24) plotted against MAAT.

Changes in Ratio 1, Ratio 2 and IR_{brGMGT} in the Lake Challa core sediments may reflect changes in MAAT in the past. Reconstructing temperature at a Lake Challa during the last interglacial from the three indices, however, provides widely different results (Fig. 36). This is perhaps not surprising given the range of %GMGT in Lake Challa itself was larger than in the East African lake data set which spans a large range of temperatures. Interestingly, in the plot of %GMGT versus time for the Lake Challa sediments (Fig. 32) a period of higher %GMGT, occurring 126 to 115 ka, corresponds to MIS5e. It is possible that the increase in brGMGTs relative to brGDGTs during MIS5e is related to an increase of temperatures in Eastern Equatorial African. More research into the environmental controls on GMGTs in lakes is needed to draw a concrete inferences about the relationship between the distribution of GMGTs and temperature in the past.

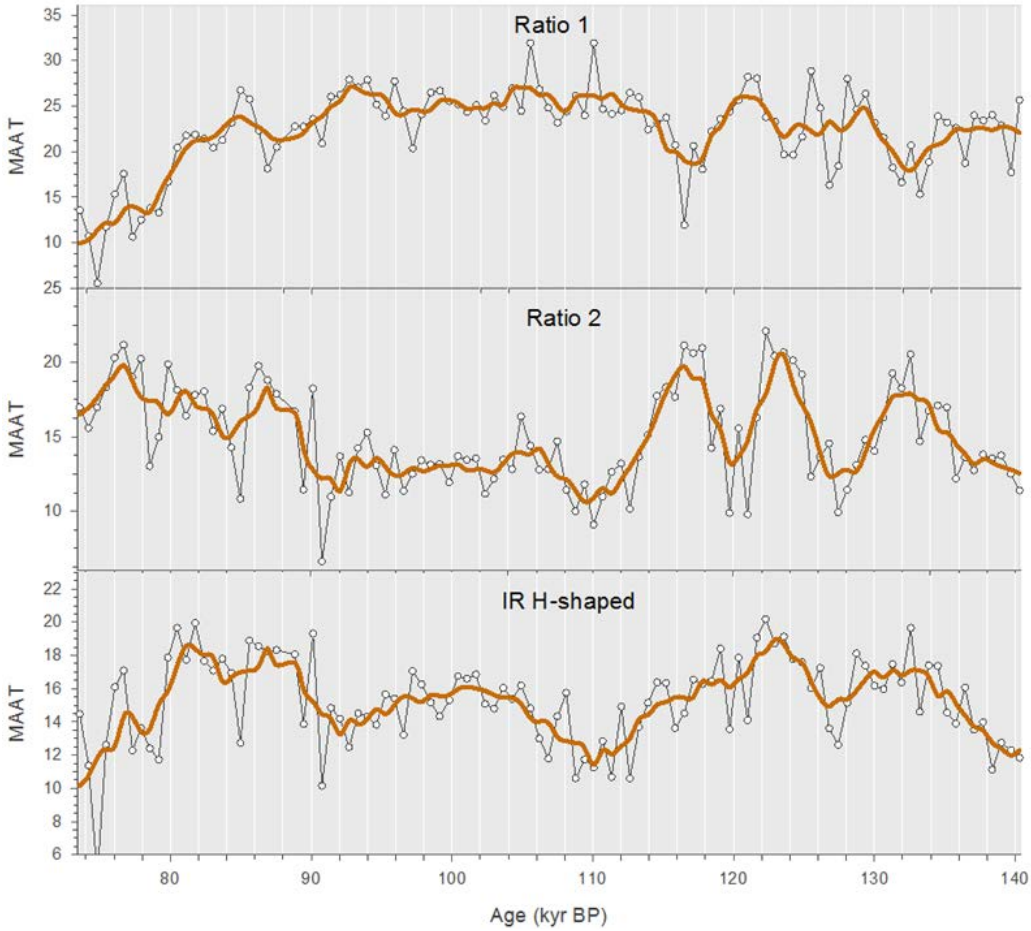

Figure 36. MAAT reconstructions for Lake Challa based on the ratios of brGMGTs described in Equations 20-25. Open circles are individual data points and the orange lines are 5 point moving averages.

5. Conclusion

The last interglacial period in Eastern Equatorial Africa was characterized by intense and prolonged episodes of aridity which is captured by the variation of the BIT record at Lake Challa. The concentration of crenarchaeol displayed a negative correlation with the BIT index, and it appears that the productivity of *Thaumarchaeota* is mainly responsible for the correspondence of the BIT index to paleoprecipitation. 'Megadroughts' occurred at Lake Challa from 138 ka to 128 ka, and from 118 to 80 ka. The first dry interval correspond to the MIS6 glaciation and the second dry interval occurred during MIS5. The length of the MIS5 megadrought recorded by the BIT index is 20 kyrs longer than indicated by seismic reflection data. Changes between arid and wet climates took place rapidly and likely had a huge impact on the ecology of the region. The possible congruence of megadroughts at Lake Challa at the equator and Lake Malawi in the southern tropics would imply that the megadroughts are not the sole result of an amplified precession cycle over this interval.

The use of TEX_{86} to estimate temperatures at Lake Challa was problematic due to the unique behaviour of the isoGDGTs and likely led to a significant underestimation of temperature. Based on distribution of brGDGTs, MIS5e was a relatively warm period at Lake Challa. Peak temperatures, of around 24°C, were reached at 135 ka, several thousand years before the onset of MIS5e. Temperature changes at Lake Challa show a similar trend to climatic variability recorded in the Antarctic Ice sheets during this interval.

brGMGTs appear abundantly in Lake Challa and are also found in lakes throughout Eastern Africa. Based on the findings of this study and previous research, brGMGTs appear to be an adaptation to warmer climates. brGMGTs hold potential as paleoclimate indicators, and several indices were developed from the East African lake data which show a strong correlation to MAAT. When applied to Lake Challa however, Ratio 1, Ratio 2 and IR_{brGMGT} result in very different temperature estimates. If the abundance of brGMGTs in Lake Challa is controlled directly by temperature variation we would not expect such a large range in %brGMGT throughout the time series (3.5% to 42.6%) which is larger than the range displayed over the entire East African lake data set (0.5% to 32%). In East African lakes with a MAAT above 20°C, there is a large scatter in the %GMGT and the fractional abundance of the individual brGMGT isomers recorded. Therefore, indices based on brGMGTs may not be suitable for reconstructing temperature variability in tropical lakes, due to the large scatter of data points at higher temperatures, which suggest that other factor besides temperature also have a significant influence on the relative abundance of brGMGTs.

Acknowledgements

I would like to thank my supervisor Jaap Sinninghe Damsté for his guidance and Ellen Hopmans for her time and support. I would further like to thank Karsten Dekker for his patience and company in the lab and Jort Ossebar for helping me with many questions. I would also like to thank Dirk Verschuren for his help.

I would like to thank my friends Jana for her help with proof reading, and Shannon for her company in the library. <3

References

Bauersachs, T and Schwark, L. 2016. Glycerol monoalkanediol diethers: a novel series of archaeal lipids detected in hydrothermal environments. *Rapid Communications in Mass Spectrometry* 30(1): 54-60.

Beuning, K., Talbot, M. and Kelts, K., 1997. A revised 30,000-year paleoclimatic and paleohydrologic history of Lake Albert, East Africa. *Palaeogeography, Palaeoclimatology and Palaeoecology* 136: 259-279

Blaga, C., Reichart, G., Heiri, O. and Sinninghe Damsté, J., 2009. Tetraether membrane lipid distributions in lake particulate matter and sediments: a study of 47 European lakes along a northesouth transect. *Journal of Paleolimnology* 41, 523-540.

Blaga, C., Reichart, G., Schouten, S., Lotter, A.F., Werne, J., Kosten, S., Mazzeo, N., Lacerot, G., and Sinninghe Damsté, J. 2010. Branched glycerol dialkyl glycerol tetraethers in lake sediments: can they be used as temperature and pH proxies? *Organic Geochemistry* 41, 1225–1234.

Blome, M., Cohen, A., Tryon, C., Brooks, A. and Russell, J. 2012. The environmental context for the origins of modern human diversity: A synthesis of regional variability in African climate 150,000–30,000 years ago. Journal of Human Evolution 62(5): 563-592.

Buckles, L., Villanueva, L., Weijers, J., Verschuren, D. and Sinninghe Damsté, J. 2013. Linking isoprenoidal GDGT membrane lipid distributions with gene abundances of ammonia-oxidizing *Thaumarchaeota* and uncultured crenarchaeotal groups in the water column of a tropical lake (Lake Challa, East Africa). *Environmental Microbiology* 15(9): 2445-2462.

Buckles, L., Weijers, J., Verschuren, D. and Sinninghe Damsté, J. 2014. Sources of core and intact branched tetraether membrane lipids in the lacustrine environment: Anatomy of Lake Challa and its catchment, equatorial East Africa. *Geochimica et Cosmochimica Acta* 140: 106-126.

Buckles, L., Verschuren, D., Weijers, J., Cocquyt, C., Blaauw, M. and Sinninghe Damsté, J. 2016. Interannual and (multi-) decadal variability in the sedimentary BIT index of Lake Challa, East Africa, over the past 2200 years: assessment of the precipitation proxy. *Climate of the Past* 12(5): 1243-1262.

Burnett, A., Soreghan, M., Scholz, C. and Brown, E. 2011. Tropical East African climate change and its relation to global climate: a record from Lake Tanganyika, Tropical East Africa, over the past 90+ kyr. *Palaeogeography, Palaeoclimatology, Palaeoecology* 303(1-4): 155-167.

Castañeda, I., Werne, J., Johnson, T. and Filley, T. 2009. Late Quaternary vegetation history of southeast Africa: The molecular isotopic record from Lake Malawi. Palaeogeography, *Palaeoclimatology and Palaeoecology* 275: 100-112.

Castañeda, I., Schefuß, E., Pätzold, J., Sinninghe Damsté, J., Weldeab, S. and Schouten, S. 2010. Millennial-scale sea surface temperature changes in the eastern Mediterranean (Nile River Delta region) over the last 27,000 years. *Paleoceanography and Paleoclimatology* 25: 1-13.

Castañeda, I. and Schouten, S. 2011. A review of molecular organic proxies for examining modern and ancient lacustrine environment. *Quaternary Science Reviews* 30. 2851-2891.

Castañeda, I and Schouten, S. 2015. Corrigendum to “A review of molecular organic proxies for examining modern and ancient lacustrine environments” [Quat. Sci. Rev. 30 (2011) 2851–2891]. Quaternary Science Reviews 125: 174-176.

Cohen, A., Stone, J., Beuning, K., Park, L., Reinthal, P., Dettman, D., Scholz, C., Johnson, T., King, J., Talbot, M., Brown, E. and Ivory, S. 2007. Ecological consequences of early Late Pleistocene megadroughts in tropical Africa. PNAS 104 (42): 16422-16427.

Costa, K., Russell, J., Konecky, B. and Lamb, H. 2014. Isotopic reconstruction of the African Humid Period and Congo Air Boundary migration at Lake Tana, Ethiopia. Quaternary Science Reviews 83: 58-67.

De Jonge, C., Hopmans, E., Zell, C., Kim, J., Schouten, S. and Sinninghe Damsté, J. 2014a. Occurrence and abundance of 6-methyl branched glycerol dialkyl glycerol tetraethers in soils: Implications for palaeoclimate reconstruction. *Geochimica et Cosmochimica Acta* 141, 97-112.

De Jonge, C., Stadnitskaia, A., Hopmans, E., Cherkashov, G., Fedotov, A., and Sinninghe Damsté, J. 2014b. In situ produced branched glycerol dialkyl glycerol tetraethers in suspended particulate matter from the Yenisei River, Eastern Siberia. Geochimica et Cosmochimica Acta 125: 476-491.

Di, H., Cameron, K., Shen, J., Winefield, C, O'callaghan, M., Bowatte, S. and He, J. 2009. Nitrification driven by bacteria and not archaea in nitrogen-rich grassland soils. Nature Geoscience, 2(9): 621-624.

Fawcett, P.J., Werne, J.P., Anderson, R.S., Heikoop, J.M., Brown, E.T., Berke, M.A., Smith, S.J., Goff, F., Donohoo-Hurley, L., Cisneros-Dozal, L.M., Schouten, S., Sinninghe Damste´, J.S., Huang, Y.S., Toney, J., Fessenden, J., WoldeGabriel, G., Atudorei, V., Geissman, J.W., Allen, C.D., 2011. Extended megadroughts in the southwestern United States during Pleistocene interglacials. *Nature* 470, 518–521.

Felton, A., Russell, J., Cohen, A., Baker, M., Chesley, J., Lezzar, K., McGlue, M., Pigati, J., Quade, J., Stager, J., Tierceline, J. 2007. Paleolimnological evidence for the onset and termination of glacial aridity from Lake Tanganyika, Tropical East Africa. *Palaeogeography, Palaeoclimatology and Palaeoecology* 252: 405-423.

Folland, C. Coauthors, 2001: Observed climate variability and change. Climate Change 2001: The Scientific Basis, JT Houghton et al., Eds.

Grove, M., Lamb, H., Roberts, H., Davies, S., Marshall, M., Bates, R. and Huws, D. 2015. Climatic variability, plasticity, and dispersal: A case study from Lake Tana, Ethiopia. *Journal of Human Evolution* 87, 32-47.

Hopmans, E., Weijers, J., Schefuß, E., Herfort, L., Sinninghe Damste, J. and Schouten, S. 2004. A novel proxy for terrestrial organic matter in sediments based on branched and isoprenoid tetraether lipids. Earth and Planetary Science Letters, 224(1-2):107-116.

Hopmans, E.,Schouten, S. and Sinninghe Damsté, J. 2016. The effect of improved chromatography on GDGT-based palaeoproxies. *Organic Geochemistry* 93: 1-6.

Huguet, C., Hopman, E., Febo-Ayala, W., Thompson, D., Sinninghe Damsté, J. and Schouten, S. 2006. An improved method to determine the absolute abundance of glycerol dibiphytanyl glycerol tetraether lipids. *Organic Geochemistry* 37: 1036-1041.

Jaeschke, A., Jørgensen, S., Bernasconi, S., Pedersen, R., Thorseth, I. and Früh-Green, G. 2012. Microbial diversity of Loki's Castle black smokers at the Arctic Mid-Ocean Ridge. *Geobiology* 10(6): 548-561.

Johnson, T., Werne, J., Brown, E., Abbott, A., Berke, M., Steinman, B.A., Halbur, J., Contreras, S., Grosshuesch, S., Deino, A. and Scholz, C. 2016. A progressively wetter climate in southern East Africa over the past 1.3 million years. *Nature* 537(7619): 220-224.

Knappy, C., Chong, J. and Keely, B. 2009. Rapid Discrimination of Archaeal Tetraether Lipid Cores by Liquid Chromatography–Tandem Mass Spectrometry. Journal of the American Society for Mass Spectrometry 20: 51-59.

Knappy, C.S., Nunn, C.E., Morgan, H.W., and Keely, B.J. 2011. The major lipid cores of the archaeon Ignisphaera aggregans: implications for the phylogeny and biosynthesis of glycerol monoalkyl glycerol tetraether isoprenoid lipids. *Extremophiles* 15:517–528.

Knappy, C., Barillà, D., Chong, J., Hodgson, D., Morgan, H., Suleman, M., Tan, C., Yao, P. and Keely, B. 2015. Mono-, di- and tri-methylated homologues of isoprenoid tetraether lipid cores in archaea and environmental samples: mass spectrometric identification and significance. Journal of Mass Spectrometry 50 (12): 1420-1432.

Kim, J., van der Meer, J., Schouten, S., Helmke, P., Willmott, V., Sangiorgi, F., Koç, N., Hopmans, E. and Sinninghe Damsté, J. 2010. New indices and calibrations derived from the distribution of crenarchaeal isoprenoid tetraether lipids: Implications for past sea surface temperature reconstructions. *Geochimica et Cosmochimica Acta* 74 (16): 4639-4654.

Lane, C., Chorn, B. and Johnson, T. 2013. Ash from the Toba supereruption in Lake Malawi shows no volcanic winter in East Africa at 75 ka. *Proceedings of the National Academy of Sciences* 110(20): 8025-8029.

Lisiecki, L. and Raymo, M. 2005. A Pliocene-Pleistocene stack of 57 globally distributed benthic d18O records. Paleoceanography 20, PA1003.

Liu, X., Summons, R. and Hinrichs, K. 2012. Extending the known range of glycerol ether lipids in the environment: structural assignments based on tandem mass spectral fragmentation patterns. Rapid Communications in Mass Spectrometry 26: 2295-2302.

Loomis, S., Russell, J and Sinninghe Damste´, J. 2011. Distributions of branched GDGTs in soils and lake sediments from western Uganda: implications for a lacustrine paleothermometer. *Organic Geochemistry* 42, 739–751.

Loomis, S., Russell, J., Ladda, B., Street-Perrott, F. and Sinninghe Damsté, J. 2012. Calibration and application of the branched GDGT temperature proxy on East African lake sediments. *Earth and Planetary Science Letters* 357–358, 277-288.

Lorius, C., Jouzel, J., Ritz, C., Merlivat, L., Barkov, N., Korotkevitch, Y. and Kotlyakov, V. 1995. A 150,000-year climatic record from Antarctic ice. *Nature* 316:591-596.

Lyons, R., Scholz, C., Cohen, A., King, J., Brown, E., Ivory, S., Johnson, T., Deino, A., Reinthal, P., McGlue, M. and Blome, M. 2015. Continuous 1.3-million-year record of East African hydroclimate, and implications for patterns of evolution and biodiversity. *Proceedings of the National Academy of Sciences* 112(51): 15568-15573.

Moernaut, J., Verschuren. D., Charlet, F., Kristen, I., Fagot, M., De Batist, M. 2010. The seismic-stratigraphic record of lake-level fluctuations in Lake Challa: Hydrological stability and change in equatorial East Africa over the last 140 kyr. *Earth and Planetary Science Letters* 209: 214-223.

Morii, H., Eguchi, T., Nishihara, M., Kakinuma, K., Konig, H. and Kogaa, Y. 1998. A novel ether core lipid with H-shaped C-80-isoprenoid hydrocarbon chain from the hyperthermophilic methanogen Methanothermus fervidus. *Biochimica et Biophysica Acta (BBA) - Lipids and Lipid Metabolism* 1390(3): 339-345.

Morrissey, A and Scholz, C. 2014. Paleohydrology of Lake Turkana and its influence on the Nile River system. *Palaeogeography, Palaeoclimatology and Palaeoecology* 403: 88-100.

Naafs, B., McCormick, D., Inglis, G., Pancost, R. and the T-GRES peat database collaborators. 2018. Archaeal and bacterial H-GDGTs are abundant in peat and their relative abundance is positively correlated with temperature. Geochimica et Cosmochimica Acta 227: 156-170.

Otto-Bliesner, B., Marshall, S., Overpeck, J. Miller, G., Hu, A. and CAPE Last Interglacial Project members. 2006. Simulating Arctic Climate Warmth and Icefield Retreat in the Last Interglaciation. Science 311: 1751-1753.

Pearson, E., Juggins, S., Talbot, H., Weckström, J., Rosén, P., Ryves, D., Roberts, S. and Schmidt, R. 2011. A lacustrine GDGT-temperature calibration from the Scandinavian Arctic to Antarctic: renewed potential for the application of GDGT-paleothermometry in lakes. *Geochimica et Cosmochimica Acta,* 75(20): 6225-6238.

Peterse, F., Prins, M.A., Beets, C.J., Troelstra, S.R., Zheng, H., Gu, Z., Schouten, S., Sinninghe Damste´, J.S., 2011. Decoupled warming and monsoon precipitation in East Asia over the last deglaciation. Earth and Planetary Science Letters 301, 256–264.

Peterse, F., van der Meer, J., Schouten, S., Weijers, J., Fierer, N., Jackson, R., Kim, J. and Sinninghe Damsté, J. 2012. Revised calibration of the MBT–CBT paleotemperature proxy based on branched tetraether membrane lipids in surface soils. *Geochimica et Cosmochimica Acta* 96: 215-229.

Pitcher, A., Hopmans, E., Mosier, A., Park, S., Rhee, S., Francis, C., Schouten, S. and Sinninghe Damsté, J. 2011. Core and Intact Polar Glycerol Dibiphytanyl Glycerol Tetraether Lipids of Ammonia-Oxidizing Archaea Enriched from Marine and Estuarine Sediments. *Applied and Environmental Microbiology* 77(10): 3468-3477.

Powers, L., Werne, J., Johnson, T., Hopmans , E., Sinninghe Damsté, J., Schouten, S. 2004. Crenarchaeotal membrane lipids in lake sediments: A new paleotemperature proxy for continental paleoclimate reconstruction? Geology 32 (7): 613-616

Powers, L., Johnson, T., Werne, J., Castañeda, I., Hopmans, E., Sinninghe Damsté, J. and Schouten, S. 2005. Large temperature variability in the southern African tropics since the Last Glacial Maximum. Geophysical Research Letters 32.

Powers, L., Werne, J., Vanderwoude, A., Johnson, T., Hopmans , E., Sinninghe Damsté, J. and Schouten, S. 2010. Applicability and calibration of the TEX86 paleothermometer in lakes. Organic Geochemistry 41, 404-413.

Powers et al 2011. Organic geochemical records of environmental variability in Lake Malawi during the last 700 years, Part I: The TEX86 temperature record.

Russell, J., Hopmans, E., Loomis, S., Liang, J., Sinninghe Damsté, J. 2018. Distributions of 5- and 6-methyl branched glycerol dialkyl glycerol tetraethers (brGDGTs) in East African lake sediment: Effects of temperature, pH, and new lacustrine paleotemperature calibrations. *Organic Geochemistry* 117, 56–69.

Saraswat, R., Nigam, R., Weldeab, S., Mackensen, A. and Naidu, P. 2005. A first look at past sea surface temperatures in the equatorial Indian Ocean from Mg/Ca in foraminifera. *Geophysical Research Letters* 32(24):1-4.

Scholz, C., King, J., Ellis, G., Swart, P., Stager, J. and Colman, S. 2003. Paleolimnology of Lake Tanganyika, East Africa, over the past 100 kyr. *Journal of Paleolimnology* 30: 139-15.

Scholz, Christopher A., Thomas C. Johnson, Andrew S. Cohen, John W. King, John A. Peck, Jonathan T. Overpeck, Michael R. Talbot et al. 2007. East African megadroughts between 135 and 75 thousand years ago and bearing on early-modern human origins. *Proceedings of the National Academy of Sciences* 104: 16416-16421.

Scholz, C., Cohen, A., Johnson, T., King, J., Talbot, M. and Brown, E. 2011. Scientific drilling in the Great Rift Valley: The 2005 Lake Malawi Scientific Drilling Project — An overview of the past 145,000 years of climate variability in Southern Hemisphere East Africa. *Palaeogeography, Palaeoclimatology and Palaeoecology* 303: 3-19.

Schouten, S., Hopmans, E., Schefuß, E. and Sinninghe Damsté, J. 2002. Distributional variations in marine crenarchaeotal membrane lipids: a new tool for reconstructing ancient sea water temperatures? *Earth and Planetary Science Letters* 204(1-2): 265-274.

Schouten, S., Huguet, C., Hopmans, E., Kienhuis, M. and Sinninghe Damsté, J. 2007. Analytical Methodology for TEX_{86} Paleothermometry by High-Performance Liquid Chromatography/Atmospheric Pressure Chemical Ionization-Mass Spectrometry. Analytical Chemistry 79: 2940–2944.

Schouten, S., Baas, M., Hopmans, E.C., Reysenbach, A. L. and Sinninghe Damsté, J.S. 2008. Tetraether membrane lipids of Candidatus "Aciduliprofundum boonei", a cultivated obligate thermoacidophilic euryarchaeote from deep-sea hydrothermal vents. *Extremophiles* 12(1): 119–124.

Schouten, S., Hopmans, E., van der Meer, J., Mets, A., Bard, E., Bianchi, T., Diefendorf, A., Escala, M., Freeman, K., Furukawa, Y. and Huguet, C. 2009. An interlaboratory study of TEX_{86} and BIT analysis using high-performance liquid chromatography–mass spectrometry. *Geochemistry, Geophysics, Geosystems 10*(3): 1-13.

Schouten, S., Hopmans, E. and Sinninghe Damsté, J. 2013. The organic geochemistry of glycerol dialkyl glycerol tetraether lipids: a review. *Organic geochemistry*, 54: 19-61.

Sinninghe Damste´, J., Ossebaar, J., Abbas, B., Schouten, S. and Verschuren, D. 2009. Fluxes and distribution of tetraether lipids in an equatorial African lake: constraints on the application of the TEX_{86} palaeothermometer and BIT index in lacustrine settings. *Geochimica et Cosmochimica Acta* 73, 4232–4249.

Sinninghe Damsté, J., Rijsptraa, W., Hopmans, E., Weijers, J., Foesel, B., Overmann, J. and Dedysh S. 2011. 13,16-dimethyl octacosanedioic acid (iso-diabolic acid), a common membrane-spanning lipid of Acidobacteria subdivi- sions 1 and 3. *Applied and Environmental Microbiology* 77, 4147–4154.

Sinninghe Damsté, J., Ossebaar, J., Schouten, S. and Verschuren, D. 2012a. Distribution of tetraether lipids in the 25-ka sedimentary record of Lake Challa: extracting reliable TEX86 and MBT/CBT palaeotemperatures from an equatorial African lake. *Quaternary Science Reviews* 50: 43-54.

Sinninghe Damsté, J., Rijpstra, W., Hopmansa, E., Jung, M., Kim, J., Rhee, S., Stieglmeier, C. and Schleper, C. 2012b. Intact Polar and Core Glycerol Dibiphytanyl Glycerol

Tetraether Lipids of Group I.1a and I.1b *Thaumarchaeota* in Soil. *Applied and Environmental Microbiology* 78: 6866-6874.

Sinninghe Damsté, J. and Verschuren, D. Unpublished. Reconstruction of temperature variability at Lake Challa over the last 250,000 years using the distribution of brGDGTs.

Sollich, M., Yoshinaga M.Y., Häusler, S., Price R.E., Hinrichs, K.U. and Bühring S.I. 2017. Heat Stress Dictates Microbial Lipid Composition along a Thermal Gradient in Marine Sediments. *Frontiers in Microbiology* 8: 1550.

Stager, J., Cumming, B., and Meeker, L. 1997. A High-Resolution 11,400-Yr Diatom Record from Lake Victoria, East Africa. *Quaternary Research* 47: 81-89.

Tierney, J. and Russell, J. 2009. Distributions of branched GDGTs in a tropical lake system: implications for lacustrine application of the MBT/CBT paleoproxy. *Organic Geochemistry* 40, 1032–1036.

Tierney, J.E., Mayes, M.T., Meyer, N., Johnson, C., Swarzenski, P.W., Cohen, A.S., Russell, J.M., 2010a. Late-twentieth-century warming in Lake Tanganyika unprecedented since AD 500. *Nature Geoscience* 3, 422-425.

Tierney, J., Russell, J., Eggermont, H., Hopmans, E., Verschuren, D., and Sinninghe Damste´, J. 2010b. Environmental controls on branched tetraether lipid distributions in tropical East African lake sediments. *Geochimica et Cosmochimica* 74, 4902–4918.

Tierney, J., Russell, J., Sinninghe Damsté, J., Huang, Y. and Verschuren, D. 2011. Late Quaternary behavior of the East African monsoon and the importance of the Congo Air Boundary. *Quaternary Science Reviews* 30, 798-807.

Tierney, J., Schouten, S., Pitcher, A., Hopmans, E. and Damsté, J. 2012. Core and intact polar glycerol dialkyl glycerol tetraethers (GDGTs) in Sand Pond, Warwick, Rhode Island (USA): insights into the origin of lacustrine GDGTs. *Geochimica et Cosmochimica Acta*, *77*: 561-581.

Tierney, J., Smerdon, J., Anchukaitis, K. and Seager, R. 2013. Multidecadal variability in East African hydroclimate controlled by the Indian Ocean. *Nature* 493(7432): 389-392.

Tierney, J. and Zander, P. 2017. A climatic context for the out-of-Africa migration. *Geology* 45(11): 1023-1026.

Verschuren, D., Sinninghe Damsté, J., Moernaut, J., Kristen, I., Blaauw, M., Fagot, M., Haug, G., van Geel, B., De Batist, M., Barker, P. and Vuille, M. 2009. Half-precessional dynamics of monsoon rainfall near the East African Equator. *Nature* 462(7273): 637-641.

Verschuren, D., Olago, D., Rucina, S. and Odhengo, P. 2013. DeepCHALLA: Two Glacial Cycles of Climate and Ecosystem Dynamics from Equatorial East Africa. Scientific Drilling 15: 72-76.

Weber, Y., De Jonge, C.,.Rijpstra, W., Hopmans, E., Stadnitskaia, A., Schubert, C., Lehmann, M., Sinninghe Damsté, J. and Niemann, H. 2015. Identification and carbon isotope composition of a novel branched GDGT isomer in lake sediments: Evidence for lacustrine branched GDGT production. *Geochimica et Cosmochimica Acta* 154, 118-129.

Weijers, J., Schouten, S., Hopmans, E., Geenevasen, J., David, O., Coleman, J., Pancost, R. and Sinninghe Damsté, J. 2006a. Membrane lipids of mesophilic anaerobic

bacteria thriving in peats have typical archaeal traits. *Environmental Microbiology* 8(4): 648-657.

Weijers, J., Schouten, S., Spaargaren, O. and Sinninghe Damsté, J. 2006b. Occurrence and distribution of tetraether membrane lipids in soils: Implications for the use of the TEX86 proxy and the BIT index. *Organic Geochemistry* 37, 1680-1693.

Weijers, J., Schouten, S., van den Donker, J., Hopmans, E., and Sinninghe Damsté, J. 2007a. Environmental controls on bacterial tetraether membrane lipid distribution in soils. *Geochimica et Cosmochimica Acta* 71, 703-713.

Weijers, J., Schefuß, E., Schouten, S. and Sinninghe Damsté, J. 2007b. Coupled thermal and hydrological evolution of tropical Africa over the last deglaciation. *Science* 315(5819): 1701-1704.

Wolff, C., Haug, G., Timmermann, A., Sinninghe Damsté, J., Brauer, A., Sigman, D., Cane, M. and Verschuren, D. 2011. Reduced interannual rainfall variability in East Africa during the last ice age. *Science* 333(6043): 743-747.

Zell, C., Kim, J., Moreira-Turcq, P., Abril, G., Hopmans, E., Bonnet, M., Lima Sobrinho, R. and Sinninghe Damsté, J. 2013. Disentangling the origins of branched tetraether lipids and crenarchaeol in the lower Amazon River: Implications for GDGT-based proxies. *Limnology and Oceanography* 58: 343-353.

Appendix 1

	Sample name	Depth (m)	Age (kyr BP)	BIT	conc. cren. (ng/g)	%H-Shaped
1	DCH-CHL16-1B-20H-3 (2.5-4.5)	60.08	73.56	0.51	5.14E+05	24.70
2	DCH-CHL16-1B-20H-3 (60-62)	60.56	74.19	0.70	1.75E+04	18.78
3	DCH-CHL16-1B-20H-3 (108-110)	61.04	74.81	0.99	7.21E+03	26.42
4	DCH-CHL16-1A-22H-2 (50.5-52.5)	61.52	75.42	1.00	X	16.05
5	DCH-CHL16-1B-21H-1 (28.5-30.5)	62.00	76.05	0.76	2.67E+04	17.97
6	DCH-CHL16-1B-21H-2 (7-9)	62.49	76.69	0.82	2.87E+04	17.75
7	DCH-CHL16-1B-21H-2 (65-67)	62.96	77.30	1.00	1.31E+03	25.90
8	DCH-CHL16-1B-21H-3 (33.5-35.5)	63.44	77.92	0.92	1.38E+04	20.45
9	DCH-CHL16-1A-23H-1 (41-43)	63.92	78.54	0.93	6.01E+03	7.93
10	DCH-CHL16-1A-23H-2 (32-34)	64.40	79.18	0.77	1.05E+05	14.83
11	DCH-CHL16-1B-22H-1 (19-21)	64.88	79.83	0.30	1.58E+05	11.72
12	DCH-CHL16-1B-22H-1 (67-69)	65.36	80.47	0.29	1.06E+05	6.93
13	DCH-CHL16-1B-22H-1 (115-117)	65.84	81.11	0.13	1.64E+05	9.65
14	DCH-CHL16-1B-22H-2 (16.5-18.5)	66.32	81.75	0.22	1.22E+05	8.33
15	DCH-CHL16-1B-22H-2 (64.5-66.5)	66.80	82.40	0.10	6.83E+04	16.01
16	DCH-CHL16-1B-22H-2 (112.5-114.5)	67.28	83.04	0.12	1.80E+05	6.86
17	DCH-CHL16-1A-24H-2 (52-54)	67.76	83.69	0.27	3.40E+04	10.69
18	DCH-CHL16-1B-23H-1 (34.5-36.5)	68.24	84.33	0.13	1.14E+05	8.73
19	DCH-CHL16-1B-23H-1 (82.5-84.5)	68.72	84.97	0.08	1.78E+05	3.53
20	DCH-CHL16-1B-23H-1 (130.5-132.5)	69.20	85.62	0.09	1.77E+05	7.42

21	DCH-CHL16-1B-23H-2 (28-30)	69.68	86.26	0.10	1.53E+05	9.84
22	DCH-CHL16-1B-23H-3 (9-11)	70.16	86.90	0.18	1.03E+05	16.71
23	DCH-CHL16-1B-23H-3 (57.5-59.5)	70.64	87.55	0.10	1.44E+05	15.61
24	DCH-CHL16-1B-24H-1 (48-50)	71.60	88.83	0.23	1.85E+05	15.42
25	DCH-CHL16-1B-24H-1 (95-97)	72.07	89.46	0.07	9.56E+04	8.19
26	DCH-CHL16-1B-24H-1 (144.5-146.5)	72.56	90.12	0.17	4.33E+04	16.40
27	DCH-CHL16-1B-24H-2 (43-45)	73.04	90.76	0.18	5.46E+04	9.10
28	DCH-CHL16-1B-24H-2 (91-93)	73.52	91.41	0.10	1.59E+05	7.36
29	DCH-CHL16-1A-26H-2 (47-49)	74.00	92.05	0.10	1.28E+05	4.67
30	DCH-CHL16-1B-25H-1 (14-16)	74.48	92.69	0.13	1.13E+05	4.74
31	DCH-CHL16-1B-25H-1 (62.5-64.5)	74.96	93.34	0.11	X	5.65
32	DCH-CHL16-1B-25H-1 (110.5-112.5)	75.44	93.98	0.13	1.06E+05	5.36
33	DCH-CHL16-1B-25H-2 (9.5-11.5)	75.92	94.62	0.10	1.85E+05	5.84
34	DCH-CHL16-1B-25H-2 (57.5-59.5)	76.40	95.27	0.18	6.02E+04	7.93
35	DCH-CHL16-1B-25H-2 (105.5-107.5)	76.88	95.91	0.10	1.47E+05	6.26
36	DCH-CHL16-1A-27H-2 (53.5-57.5)	77.36	96.55	0.08	2.15E+05	7.56
37	DCH-CHL16-1A-27H-2 (103.5-105.5)	77.84	97.20	0.29	6.04E+04	13.13
38	DCH-CHL16-1A-27H-3 (41.5-43.5)	78.32	97.84	0.14	1.82E+05	4.28
39	DCH-CHL16-1A-27H-3 (89.5-91.5)	78.80	98.49	0.08	2.44E+05	7.86
40	DCH-CHL16-1A-27H-3 (137.5-139.5)	79.28	99.13	0.09	1.30E+05	7.61
41	DCH-CHL16-1A-28H-1 (17-19)	79.79	99.81	0.12	1.40E+05	7.64
42	DCH-CHL16-1A-28H-1 (62.5-64.5)	80.24	100.42	0.10	1.48E+05	10.99
43	DCH-CHL16-1A-28H-1 (111-113)	80.72	101.06	0.11	1.34E+05	7.84
44	DCH-CHL16-1B-27H-1 (43.5-45.5)	81.20	101.70	0.12	1.22E+05	5.88
45	DCH-CHL16-1B-27H-1 (91.5-93.5)	81.68	102.34	0.17	1.07E+05	5.85
46	DCH-CHL16-1B-27H-1 (139.5-141.5)	82.16	102.98	0.11	1.90E+05	9.11
47	DCH-CHL16-1B-27H-2 (45.5-47.5)	82.64	103.63	0.12	1.52E+05	7.07
48	DCH-CHL16-1A-29H-1 (43.5-45.5)	83.12	104.27	0.11	1.14E+05	7.22
49	DCH-CHL16-1A-29H-1 (91-92)	83.60	104.90	0.16	6.46E+04	12.33
50	DCH-CHL16-1B-28H-1 (26-28)	84.08	105.56	0.13	1.34E+05	7.19
51	DCH-CHL16-1B-28H-1 (74-76)	84.56	106.20	0.09	1.32E+05	5.06
52	DCH-CHL16-1B-28H-1 (122-124)	85.04	106.85	0.11	1.23E+05	5.70
53	DCH-CHL16-1B-28H-2 (24-26)	85.52	107.49	0.12	1.81E+05	7.11
54	DCH-CHL16-1B-28H-2 (72-74)	86.00	108.14	0.11	2.25E+05	3.93
55	DCH-CHL16-1B-28H-2 (120-122)	86.48	108.78	0.08	1.62E+05	4.33
56	DCH-CHL16-1A-30H-2 (61-63)	86.96	109.42	0.10	9.24E+04	6.84
57	DCH-CHL16-1B-29H-1 (41.5-43.5)	87.44	110.07	0.09	8.06E+04	6.02
58	DCH-CHL16-1B-29H-1 (91.5-93-5)	87.92	110.71	0.08	1.05E+05	6.42
59	DCH-CHL16-1B-29H-1 (139.5-141.5)	88.40	111.35	0.07	2.14E+05	8.52
60	DCH-CHL16-1B-29H-3 (2-4)	88.91	112.03	0.06	9.10E+04	14.53
61	DCH-CHL16-1A-31H-1 (25-27)	89.36	112.64	0.06	1.21E+05	6.40
62	DCH-CHL16-1A-31H-2 (12-14)	89.84	113.28	0.07	1.58E+05	6.93
63	DCH-CHL16-1A-31H-2 (62.5-64.5)	90.32	113.92	0.09	1.03E+05	9.06

64	DCH-CHL16-1B-30H-1 (53.5-55.5)	90.80	114.57	0.09	1.63E+05	8.85
65	DCH-CHL16-1B-30H-1 (104-106)	91.28	115.21	0.08	1.39E+05	10.76
66	DCH-CHL16-1B-30H-2 (3.5-5.5)	91.76	115.85	0.04	6.84E+04	18.14
67	DCH-CHL16-1B-30H-2 (52-54)	92.24	116.50	0.08	1.58E+05	30.20
68	DCH-CHL16-1B-30H-2 (99.5-101.5)	92.72	117.14	0.07	2.91E+05	14.25
69	DCH-CHL16-1A-32H-1 (92-94)	93.20	117.79	0.06	2.01E+05	18.75
70	DCH-CHL16-1B-31H-1 (15-17)	93.68	118.43	0.29	6.42E+04	13.31
71	DCH-CHL16-1B-31H-1 (63-65)	94.16	119.07	0.54	2.56E+04	19.85
72	DCH-CHL16-1B-31H-1 (111-113)	94.64	119.72	0.60	1.26E+04	16.08
73	DCH-CHL16-1B-31H-2 (44-46)	95.12	120.36	0.09	3.14E+05	15.47
74	DCH-CHL16-1B-31H-2 (92-94)	95.60	121.00	0.26	6.95E+04	15.38
75	DCH-CHL16-1A-33H-1 (59-61)	96.08	121.65	0.06	6.54E+05	13.85
76	DCH-CHL16-1A-33H-1 (107-109)	96.56	122.29	0.06	2.23E+05	20.18
77	DCH-CHL16-1B-32H-1 (44.5-46.5)	97.04	122.93	0.33	3.30E+04	27.94
78	DCH-CHL16-1B-32H-1 (97.5-99.5)	97.52	123.57	0.44	8.56E+03	42.64
79	DCH-CHL16-1A-34H-1 (8.5-10.5)	98.01	124.23	0.75	6.73E+03	29.08
80	DCH-CHL16-1A-34H-1 (55.5-57.5)	98.48	124.86	0.13	1.38E+05	19.97
81	DCH-CHL16-1A-34H-1 (103.5-105.5)	98.96	125.51	0.12	1.52E+05	8.75
82	DCH-CHL16-1A-34H-2 (41-43)	99.44	126.15	0.10	9.53E+04	16.91
83	DCH-CHL16-1B-33H-1 (19-21)	99.92	126.79	0.93	1.61E+03	15.74
84	DCH-CHL16-1B-33H-1 (68.5-70.5)	100.40	127.43	0.38	1.45E+05	9.72
85	DCH-CHL16-1B-33H-1 (116.5-118.5)	100.88	128.08	0.07	3.10E+05	7.45
86	DCH-CHL16-1A-35H-1 (26-28)	101.36	128.72	0.23	6.07E+04	12.14
87	DCH-CHL16-1A-35H-1 (78.5-80.5)	101.84	129.36	0.12	1.39E+05	11.16
88	DCH-CHL16-1A-35H-3 (33.5-35.5)	102.32	130.01	0.12	1.66E+05	14.58
89	DCH-CHL16-1A-35H-3 (81.5-83.5)	102.80	130.65	0.11	1.93E+05	9.16
90	DCH-CHL16-1B-34H-1 (120.5-122.5)	103.28	131.29	0.12	1.40E+05	21.25
91	DCH-CHL16-1A-36H-1 (27-29)	103.76	131.94	0.12	2.14E+05	19.74
92	DCH-CHL16-1A-36H-1 (79-81)	104.24	132.58	0.10	2.23E+05	16.70
93	DCH-CHL16-1A-36H-1 (127-129)	104.72	133.22	0.17	1.09E+05	12.35
94	DCH-CHL16-1A-36H-2 (25-27)	105.20	133.87	0.08	3.23E+05	11.33
95	DCH-CHL16-1B-35H-1 (49-51)	105.68	134.51	0.09	3.18E+05	7.14
96	DCH-CHL16-1B-35H-1 (101.5-103.5)	106.16	135.15	0.07	5.74E+05	8.68
97	DCH-CHL16-1C-2E-2 (115.5-117.5)	106.64	135.80	0.10	2.55E+05	13.05
98	DCH-CHL16-1C-2E-3 (30-32)	107.12	136.43	0.13	1.09E+05	12.83
99	DCH-CHL16-1C-2E-3 (78-80)	107.60	137.08	0.05	5.78E+05	6.79
100	DCH-CHL16-1C-2E-3 (127-129)	108.08	137.73	0.13	2.37E+05	10.75
101	DCH-CHL16-1B-36H-1 (63-65)	108.56	138.37	0.06	3.78E+05	6.80
102	DCH-CHL16-1B-36H-1 (118-120)	109.04	139.01	0.21	1.29E+05	9.67
103	DCH-CHL16-1C-3E-2 (2-4)	109.55	139.69	0.56	2.55E+04	9.24
104	DCH-CHL16-1C-3E-2 (58.5-60.5)	110.00	140.30	0.32	3.55E+04	11.68